Elastic Critical Buckling of T-Sections subjected to Axial or End Moment Loading

Clayton Montanaro

Dissertation submitted to the Faculty for the Built Environment, University of Malta in partial fulfillment of the requirements for the attainment of the degree of Master of Engineering (Structural Engineering)

June 2025

L-Università ta' Malta

FACULTY/INSTITUTE/CENTRE/SCHOOL Faculty for the Built Environment

DECLARATIONS BY POSTGRADUATE STUDENTS

(a) Authenticity of Dissertation

I hereby declare that I am the legitimate author of this Dissertation and that it is my original work.

No portion of this work has been submitted in support of an application for another degree or qualification of this or any other university or institution of higher education.

I hold the University of Malta harmless against any third party claims with regard to copyright violation, breach of confidentiality, defamation and any other third party right infringement.

(b) Research Code of Practice and Ethics Review Procedures

I declare that I have abided by the University's Research Ethics Review Procedures. Research Ethics & Data Protection form code BEN-2024-00112.

As a Master's student, as per Regulation 77 of the General Regulations for University Postgraduate Awards 2021, I accept that should my dissertation be awarded a Grade A, it will be made publicly available on the University of Malta Institutional Repository.

Dedicated to my loving family

Acknowledgements

Firstly, I would like to express my sincere gratitude to my supervisor, Prof. Spiridione Buhagiar B.E.&A. (Hons), M.Sc. (Lond.), D.I.C., Ph.D. (Lond.), F.I.Struct.E., M.A.S.C.E., C.Eng., Perit for his ongoing guidance and invaluable feedback throughout this academic journey.

Secondly, I would like to extend my gratitude to my colleagues, lecturers and faculty staff, all of whom made this experience immensely enriching and enjoyable.

Finally, I would like to express my heartfelt appreciation to my family, whose unwavering love and support have been instrumental throughout my studies.

Abstract

It is common practice in the industry to use universal column and beam sections for the primary structural members when designing a steel frame structure. However, flanged cruciform sections (FCS) offer various advantages over other hot-rolled column sections, especially when utilised in moment-resisting frames. Research on FCS buckling behaviour, particularly for columns under end-moment loading, is limited, and codes such as EN1993-1-1 (2005) provide no specific design guidance.

This study investigates the elastic critical buckling behaviour of the T-section undergoing compression in an FCS by introducing longitudinal web restraints to the free edge of the T-section, to simulate the web edge restraints in the FCS section. A parametric study for the elastic critical eigenvalue buckling stress was conducted using LUSAS (2024) for two different load combinations, an axial compression stress and a compression stress distribution for uniform sagging end moment bending, as well as five different web restraining support conditions. Four different cross-sections with a constant flange slenderness ratio (c_f/t_f) and varying the web slenderness ratios (c_w/t_w) in the range of 35.5 – 361.4 were analysed. The member lengths for each model were varied from 1m to 8m.

A convergence study was carried out to determine the accuracy of the chosen finite element mesh, and a comparison between theoretical and FEA elastic critical buckling stress was conducted. A good correlation was observed between the theoretical and FEA predictions. The FEA results showed that the torsional mode of buckling is the critical mode of buckling. For shorter lengths, the distortional buckling mode was observed, and this mode of buckling tended to converge to the torsional mode in the models with a higher web slenderness ratio. The distortional mode of buckling also indicated that it is more sensitive to the bending stiffness of the web than the torsional mode of buckling.

Ultimately, this study provides data for the future development of design equations that may be able to predict the elastic critical buckling load for members in compression and subjected to uniform sagging moment, thus facilitating a method for the design of FCS as well as any other compound section that consists of radiating T-sections joined together at the free end of the web.

Keywords

- T-Sections
- Flanged Cruciform Sections
- Finite Element Analysis
- Elastic Critical Buckling

Table of Contents

List of Tables

List of Figures

Glossary

The notation used in study is provided hereunder

A	Area of Cross-Section
E	Young's Modulus of Elasticity
G	Shear Modulus of Elasticity
I_z	Second Moment of Area about z-axis
I_y	Second Moment of Area about y-axis
I_w	Warping Constant
J	Torsion Constant
L	Length
M_{cr}	Elastic Critical Moment
N_{cr}	Elastic Critical Force
$N_{cr,\,y}$	Flexural Buckling load about y-axis
$N_{cr,\,z}$	Flexural Buckling load about z-axis
$N_{cr,\,T}$	Torsional Buckling Load
$N_{cr,\,FT}$	Flexural-Torsional Buckling Load
C_1	Factor depending on Loading Conditions
C_2	Factor depending on End Restraint Condition
k_z	Effective Length Factor
H	Height of Web
B	Width of Flange
t_f	Flange Thickness
t_w	Web Thickness
ρ	Material Density
r_o	Polar Radius of Gyration
ν	Poisson's Ratio
σ_o	Yield Stress
σ_{cr}	Critical Stress
z_j	Monosymmetry parameter
z_s	Shear centre coordinate with respect to centroid

The abbreviations and acronyms used in this study is provided hereunder

FCS	Flanged Cruciform Section
FE	Finite Element
FEA	Finite Element Analysis
kN	Kilonewton
kNm	Kilonewton-metre
m	Metre
mm	Millimetre
N	Newton

Chapter 1: Introduction

1.1 Background

One of the most common types of structural systems, especially in medium to high rise buildings is a steel frame structure. The structural grid of these structures typically consists of an orthogonal configuration, where the main structural elements are column and beam members. A plan of a typical frame structure is shown in Figure 1.1.

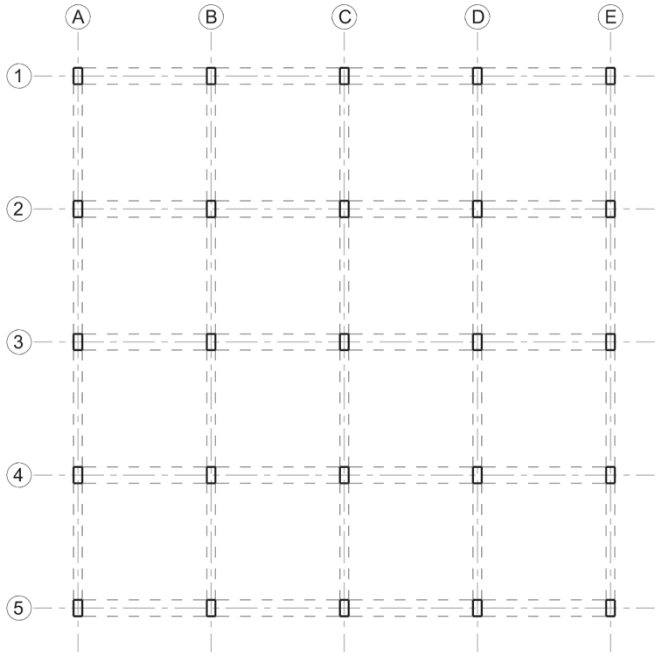

Figure 1.1 - Typical Grid Plan Layout for Frame Structure

Universal column sections are the typical cross-sections used as column members in frame structures. When these cross-sections are used, they are strategically oriented in a way such that their major axis resists the largest lateral force, which usually results from the larger span. However, when designing moment-resisting frames, it is difficult to facilitate moment connections on all four sides of a column when universal sections are used. Flanged cruciform sections (FCS), shown in Figure 1.2 are more suitable for facilitating moment connections on all four sides, apart from offering equal flexural stiffness about both axes of the column.

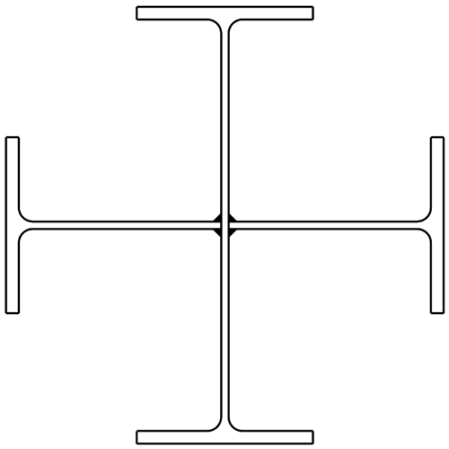

Figure 1.2 - Typical Flanged Cruciform Cross-Section

1.2 Objectives

Geometrically, an FCS is composed of four radiating T-sections, all joined at the free edge of the web. This study will discretise the cross-section by considering the T-section, which is compressed due to axial or bending moment. By doing so, it may be possible to obtain a fundamental understanding of the elastic critical behaviour of an FCS with a T-section, where longitudinal web restraints shall be introduced to simulate this behaviour.

In Figure 1.3, the two extremes for the torsional capacity of the T-sections are visualised. On the left (Figure 1.3(a)), the free edge of the web is restrained translationally and left free to rotate. On the far right (Figure 1.3(c)), the cross-section is fully restrained against rotation.

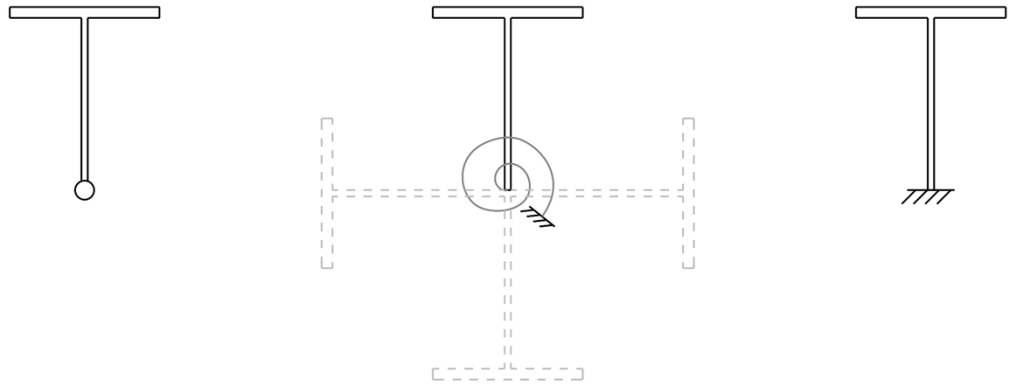

(a) (b) (c)

Figure 1.3 - Longitudinal Web Restraining Support Conditions

By understanding the behaviour of the cross-section in these cases where the T is either completely free to rotate or fully restrained against rotation, the next step would be to understand the behaviour when the T-section is restrained by the rest of the compound sections' members, i.e. the other T-sections (Figure 1.3(b)). Therefore, this theory can be extended to other cross-sections which are composed of several radiating T-sections, as shown in Figure 1.4

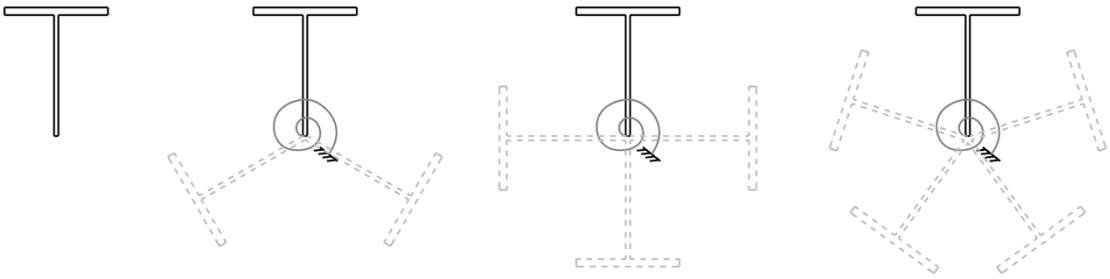

(a) (b) (c) (d)

Figure 1.4 - (a) n = 1 (b) n = 3 (c) n = 4 (d) n = 5, where n = number of T-Sections

Therefore, the main objectives of this study include:

i. Assessing the elastic critical buckling behaviour of T-sections, specifically when the flange is undergoing a compression instability, by exploring the behaviour under axial and end moment loading for varying web slenderness ratios and member lengths.

ii. The effects of web restraining support conditions on the free edge of the web shall be explored to propose an optimal model for simulating the elastic critical buckling behaviour of FCS and compound sections (Figure 1.4)

iii. Developing an approach for determining the elastic critical buckling behaviour, leading to facilitating the design of FCS as well as other compound sections, which are composed of a number of radiating T-section geometries, as shown in Figure 1.4.

1.3 Dissertation Overview

This study will consist of the following chapters: literature review, methodology, results and conclusions

Chapter 2, the Literature Review, presents an overview of the previous research and experimental data published for T-sections and FCS. The various forms of elastic buckling modes are discussed alongside the available theoretical equations for calculating the elastic critical buckling loads under compression and elastic critical moment for these cross-sections.

Chapter 3, the Methodology, describes the procedure and variables involved in the parametric study conducted. This chapter outlines the modelling process for the FE model, along with the load cases applied in the analysis, and explains the additional section properties required for use within the theoretical equations of elastic critical buckling.

Chapter 4, the Results, presents the findings of the parametric study, where the results gathered from the study are interpreted, and conclusions are drawn based on these findings are given. A comparison between the different web restraining conditions tested is also given.

Finally, Chapter 5 presents a discussion of the key findings that were made in this dissertation, along with suggestions for further research.

Chapter 2: Literature Review

2.1 Introduction

This chapter aims to review existing research on the buckling of steel T-sections and compound sections, with the aim of understanding the buckling behaviour of compound sections fabricated by welding together multiple individual T-sections (Figure 1.4).

Research and experimental data carried out on compound sections, such as shown in Figure 1.4 are not readily available. Limited research on flanged cruciform sections (FCS) has been found. It will be reviewed, with a primary focus on the elastic critical buckling behaviour of these sections when subjected to axial load, end moments, or a combination of both.

2.2 The T-Section

While T-section steel members have been employed in the building and construction industry, research on these types of members has not been as prevalent as on more commonly used sections, such as I and angle sections. These types of cross-sections are usually used as secondary members or in composite systems such as concrete deck slabs.

A steel T-section can be produced by cutting standard hot-rolled I-sections in half (Figure 2.1 (a)). However, it can also be made by plate welding two plates together (Figure 2.1 (b)) or by joining two angle sections to each other, as shown in Figure 2.1 (c).

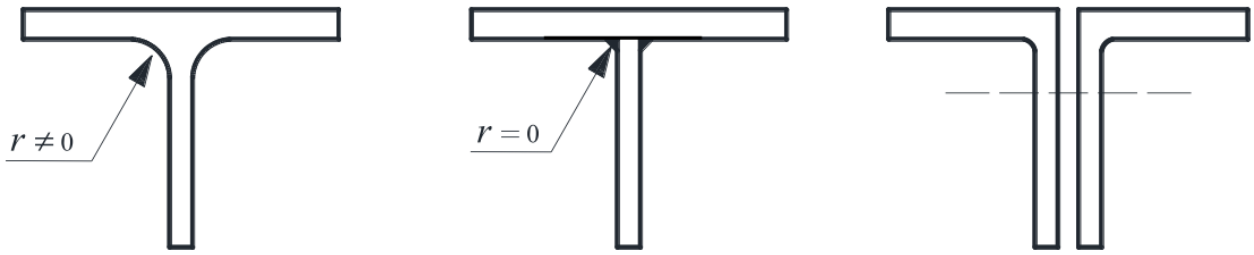

Figure 2.1 - (a) Half an I-section, (b) Plate welded, (c) Two angle sections (Li et al., 2022)

The T-section is characterised by monosymmetry about the minor axis. Given its monosymmetric nature, the centroid and the shear centre of the section are not coincident, as seen in Figure 2.2. The mid-wall centrelines of the flange and web elements intersect only at a single point, similar to angle and cruciform sections. This implies that the primary warping constant of T-section members is zero (Li et al., 2022).

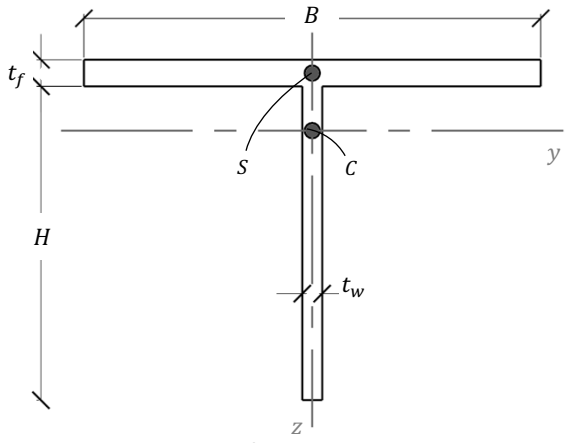

Figure 2.2 - Diagram of T-Section geometric properties

These types of cross-sections derive their warping resistance from a secondary warping constant. This indicates that these types of sections have a very low warping stiffness, making them highly susceptible to torsional buckling phenomena. In some cases, design codes such as EN 1993-1-1 (2005) neglect the effects of the secondary warping constant and assume the warping constant as zero, since the effects of it are relatively small and only seem to affect very short columns (Cardoso & Rasmussen, 2013; Li et al. 2022)

Physical experimentation of T-sections has been relatively scarce when compared to more common sections, such as I-sections and angle sections. Some of the earlier experiments conducted on T-sections were performed by (Kennedy & Murty, 1972), who tested 27 Tee struts. They proposed that the member capacity shall be determined from the minimum of the elastic critical theoretical buckling loads, namely, the local, the flexural, and flexural–torsional buckling loads.

Kitipornchai & Lee (1986) conducted a series of experimental tests and a theoretical analysis on the inelastic buckling behaviour under axial compression for single-angle, T, and double-angle sections. Results showed that for T-sections with wide flanges, the predominant mode of buckling was flexural buckling. In contrast, for members with thickness-to-width (h/b) ratios smaller than 1, the predominant mode of buckling was flexural-torsional buckling. They also conducted a comparison of the cross-section's capacity with the design recommendations of the Australian design codes. For single and double angle struts, the comparison was found to be satisfactory; however, it was slightly unconservative for the T-struts.

Dinis et al. (2010) employed Generalised Beam Theory (GBT) to perform a numerical analysis on angle, T and cruciform thin-walled members. Their results highlighted that these types of cross-sections are highly prone to torsional buckling, and sometimes it is difficult to distinguish between torsional and local buckling modes. They also noted that a rational model for T and cruciform sections shall be based on the torsional buckling behaviour rather than local buckling.

Trahair (2013) analysed the post-buckling strength of T columns with a particular focus on the torsional buckling and post-buckling behaviour. He highlighted the shortcomings of the design codes, which account separately for torsional and local buckling, resulting in a double consideration of these effects and hence leading to an overconservative design.

Taras et al. (2016) note that it is challenging to establish straightforward design rules for buckling checks of T-sections, particularly due to their unusual behaviour, with a focus on cross-sections featuring slender webs. Additionally, they also noted that for these types of sections, the local and torsional modes are often indistinguishable from each other, and they do not interact in the same manner as expected when comparing their behaviour to that of other cross-sections.

2.3 The Flanged Cruciform Section

FCS are compound sections consisting of four radiating T-sections. Typically, they are fabricated from two universal I-sections by cutting one of the I-sections in half along its longitudinal axis and attaching the resulting T-sections to the I-section using fillet welds (Figure 2.3). These cross sections are utilised in applications where considerable compression resistance is required; they are also used as bracing members and in scenarios where considerable bending moment resistance is needed about both axes (Harris & Urgessa, 2018).

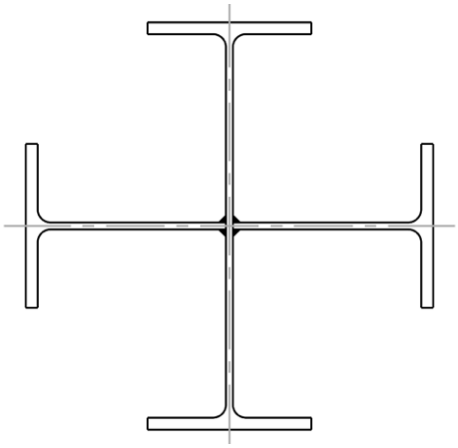

Figure 2.3 - Flanged Cruciform Cross-Section

Since FCS are point symmetric, with their shear centre and centroid coinciding, when subjected to axial loading, the critical buckling failure modes typically comprise torsional buckling for short to medium length members, and flexural buckling in long members (Dai et al., 2024).

King (2006) explains how the torsional mode is not usually the critical mode of buckling for FCS, especially when the flanges are restrained. He also explored the design recommendations as provided by British Standard design codes BS 5950:2000 and suggested two buckling curves when designing these sections for these modes.

Tahir et al. (2008) analysed the axial capacity of FCS composed of universal beam sections, comparing the theoretical axial capacity predicted by design guidelines, EN 1993-1-1 (2005), and BS 5950:2000, on a column with a slenderness ratio in the range of 26-35. The results showed that when compared to the design recommendations of EN 1993-1-1 (2005), the results showed that the actual ratio of the column's capacity fell in the range of 1.08 – 1.47. When compared to BS 5950-1:2000, the ratio was 1.01 – 1.21, which are very conservative predictions from both design codes.

Tahir et al. (2008) remarked on the numerous advantages of utilising a universal beam section for the fabrication of an FCS over a universal column section. These include an increase in axial capacity, improved stiffness about both principal axes and the facilitation of easier connection design due to the larger space between the flanges.

Naderian et al. (2019) analysed the buckling behaviour of plain and flanged cruciform sections under shear and compression loading using CFSM. They also compared the behaviour of cruciform sections to those of T, U and I-sections, where their results showed that in the local buckling region, the cruciform section, the I-section and the T-section have identical values of buckling stress. In contrast, the buckling stress in the flexural-torsional region for the I-sections and T-sections is approximately the same.

2.4 Elastic Buckling

Buckling can be defined as the structural behaviour where a structure or a structural member deforms in a plane that is not the same as the plane in which the element was loaded in (Trahair, 1993). At the member level, buckling can be categorised into three categories, that is, local, distortional, and global buckling.

The primary modes of buckling that can be observed in a T-section under axial loading are local and global buckling. Buckling behaviour is dependent on various factors, including cross-section geometry, length and boundary conditions (Schafer & Ádány, 2005).

2.4.1 Local Buckling

Local buckling refers to a buckling mode that involves individual out-of-plane deformations of plate elements (Figure 2.4(a)) and is therefore resisted by the flexural rigidity of the plate. This type of buckling typically occurs in members of short lengths, and usually the half wavelength is of the order of the plate width (Trahair, 1993).

In T-sections, local buckling is influenced by the element interaction of the plate elements with different slenderness values, which buckle locally at different critical stresses if considered in isolation. Hence, when undergoing local buckling, the slenderer plate element receives rotational restraint from the adjoining element (Gardner et al., 2019).

2.4.2 Global Buckling

The two overall modes of failure for a T-section column include a flexural mode about the major axis (Figure 2.4(b)) and a flexural-torsional mode, which consists of a coupled mode of flexure in the minor axis and torsion about the shear centre (Figure 2.2(c)).

Figure 2.4 - Buckling Modes: (a) Local buckling mode (b) Flexural buckling about major axis (c) Flexural-torsional buckling

According to classical theory of elastic instability (Timoshenko & Gere, 1963) the critical global buckling load, shall be defined as the minimum value between the two flexural buckling loads $N_{cr,y}$ and $N_{cr,z}$ as described by equations 2-1, and 2-2, and the torsional buckling load $N_{cr,T}$, equation 2-3. However, for a T-section, since the centroid and shear centre do not coincide, the flexural buckling about the z-axis and the torsional buckling mode cannot be uncoupled, and hence, the flexural-torsional buckling load $N_{cr,FT}$ is defined by equation 2-4.

Flexural buckling load about the y-axis is:

$$N_{cr,y} = \frac{\pi^2 E I_y}{L^2} \qquad (2-1)$$

Flexural buckling load about the z-axis:

$$N_{cr,z} = \frac{\pi^2 E I_z}{L^2} \qquad (2-2)$$

Torsional buckling load:

$$N_{cr,T} = \frac{1}{{r_0}^2 + {x_0}^2 + {y_0}^2}\left(GJ + \frac{\pi^2 E I_w}{L^2}\right) \qquad (2-3)$$

Flexural-torsional buckling load:

$$N_{cr,FT} = \frac{(N_{cr,z} + N_{cr,T}) \pm \sqrt{(N_{cr,z} + N_{cr,T})^2 - 4N_{cr,z} \cdot N_{cr,T} \frac{{r_0}^2}{{r_0}^2 + {y_0}^2}}}{\frac{2{r_0}^2}{{r_0}^2 + {y_0}^2}} \qquad (2-4)$$

where,

(x_0, y_0) represent the coordinates of the shear centre in the principal axis system

${r_0}^2 = \frac{I_x + I_y}{A}$ is the polar radius of gyration

L is the member length

E is the material Young's modulus

G is the material shear modulus

J is the torsion constant

I_w is the warping constant

I_y is the second moment of area, about the y-axis

I_z is the second moment of area, about the z-axis

2.5 Lateral Torsional Buckling

Lateral torsional buckling is characterised by a combined twist and lateral bending of the cross-section, shown in Figure 2.5. This is often the result of when a cross-section's out-of-plane resistance is less than its in-plane resistance. This type of buckling is particularly critical in situations where an unrestrained I-section is being designed. Research on elastic buckling is abundant for unrestrained I-section beam columns; in fact, guidelines such as (SN003b-EN-EU, 2008) are available for calculating the elastic critical moment.

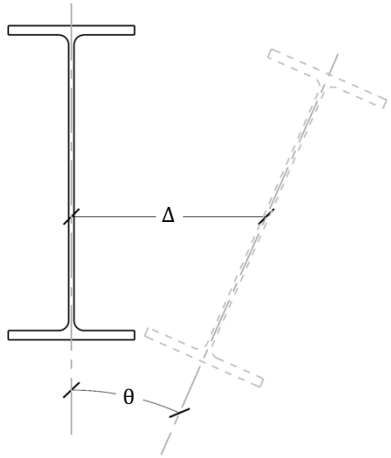

Figure 2.5 - Lateral Torsional Buckling of an I-section

2.5.1 Elastic Critical Moment

SN030a-EN-EU (2012) suggests that for a uniform cross-section symmetric about the minor axis, the elastic critical moment can be evaluated using equation 2-5:

$$M_{cr} = C_1 \frac{\pi^2 EI_z}{(k_z L)^2}\left\{\sqrt{\left(\frac{k_z}{k_w}\right)^2 \frac{I_w}{I_z} + \frac{(k_z L)^2 GJ}{\pi^2 EI_z} + (C_2 z_g - C_3 z_j)^2} - (C_2 z_g - C_3 z_j)\right\} \qquad (2-5)$$

For a T-section, under uniform end moment, the equation can be arranged to:

$$M_{cr} = C_1 \frac{\pi^2 EI_z}{(k_z L)^2}\sqrt{\frac{I_w}{I_z} + \frac{L^2 GJ}{\pi^2 EI_z} + \left(C_3 z_j\right)^2} - C_3 z_j \qquad (2-6)$$

where,

$C_1,\ C_3$ Factors depending on the loading and end restraint conditions, which can be found in Table 4.1 of the same document. For the loading being considered, $C_1 = C_3 = 1$.

k_z is the effective length factor for end rotation about the z axis = 1, for being free to rotate about the z-axis.

k_w is the effective length factor for end warping = 1, for being free to warp but restrained against rotation about the longitudinal axis.

z_j is the monosymmetry parameter and can be found using equation 2-7.

$$z_j = z_s - 0.5 \int_A (y^2 + z^2) \frac{z}{I_y} dA \qquad (2 - 7)$$

where,

z_s is the coordinate of the shear centre with respect to the centroid.

A is the area of the cross section.

The value for M_{cr} depends on the direction in which the moment is applied, whether clockwise or counterclockwise, as shown in Figure 2.6; hence there are two values for the elastic critical moment. Equation 2-6 gives the value for the lowest value for the critical moment, which is when a negative moment is applied to the ends of the member.

However, this load case causes failure due to local buckling of the web, which is outside the scope of this dissertation, which aims to assess the compression instability in the top flange. Therefore, this load case was excluded from the study.

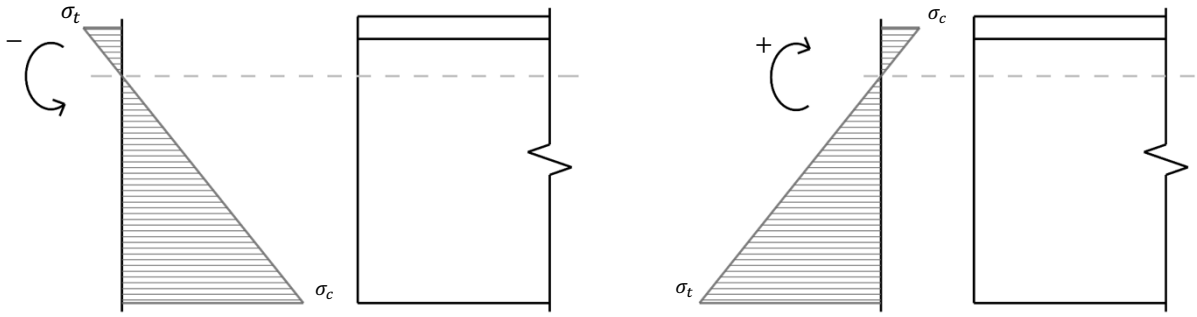

Figure 2.6 - (Left) Negative end moment, (Right) Positive end moment

A loading condition that aligns with the interest of this dissertation would be one where the top flange is subjected to compression. When a positive moment is applied at the ends, the flange is put into compression; however, given the geometry of the T-section, since the position of the neutral axis will always be closer to the flange, failure by yielding of the web will still occur before buckling of the flange.

2.6 Lateral Distortional Buckling

A distortional mode of buckling describes an intermediary mode between local and global buckling. Unlike a global buckling mode, a distortional mode results in changes to the shape of the cross-section, and it usually involves displacement of the element over a part of the member's length, rather than throughout the entire length (Trahair, 1993).

When a restrained beam-column is only braced at the tension flange as shown in Figure 2.7, the buckling mode must be distortional in nature (Bradford, 1992). Therefore, the in-plane distortion of the web occurs as a result of having to restrain the compressive flange.

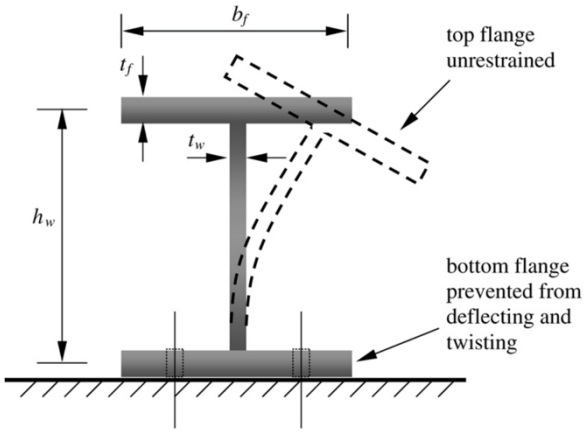

Figure 2.7 - Distortional Buckling of an I-section fully restrained on one flange (Vrcelj & Bradford, 2006)

Bradford (1997) states that for unrestrained I-sections, this mode of buckling is usually not significant; however, for partially restrained or continuously restrained I-sections, lateral distortional buckling should not be ignored. He also outlines that when the classical Vlasov-type flexural, torsional and flexural buckling is applied, the cross-section is treated as rigid, which is not a correct assumption, since for a fully restrained tension flange, Vlasov theory predicts an infinite buckling load.

Therefore, he proposes an insight into when the rigid cross-section assumption is relaxed and considers the elastic lateral-distortional buckling of a monosymmetric I-section column, with a stocky compression flange, where the tension flange is restrained elastically against twist. He then utilises the energy method of analysis to develop an eigenvalue problem and presents numerical solutions.

Vrcelj & Bradford (2006) mention that restrained distortional buckling is influenced by multiple effects, including the effects of axial loads, the distribution of moment, and slenderness at member and cross-section levels, and hence a solution is not expressible in a closed form.

Tohidi & Sharifi (2014) conducted a parametric study using the software package ABAQUS and evaluated the performance of half-through bridge girders, where the stiff deck restrains the I-sections. Figure 2.8 shows the distortional buckling mode that can be observed under these constraints. This mode was especially noticeable for girders, which consist of stocky flanges and slender webs, where it was described as an interaction between local buckling and lateral translation.

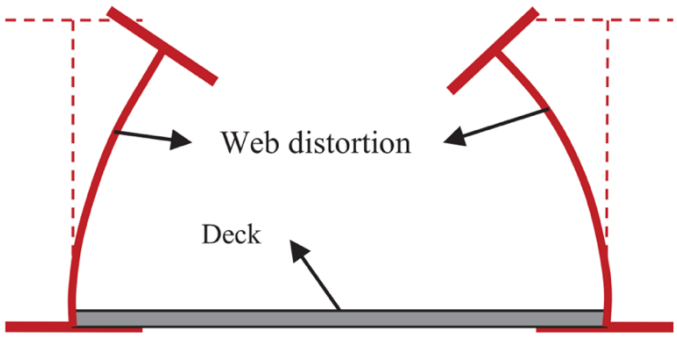

Figure 2.8 - Distortional Buckling of half-through girder bridges (Tohidi & Sharifi, 2014)

Chapter 3: Methodology

3.1 Introduction

The methodology chapter shall include an explanation of the approach adopted for carrying out this research study. It will consist of two main parts, namely the theoretical analysis, which utilises the theoretical equations described in Section 2.4.2 to carry out a numerical analysis for the elastic critical buckling loads, and the following part shall focus on the FE modelling, where a description of the process adopted, and FE model is given.

3.2 Theoretical Analysis

The section properties for the T-sections are listed alongside the classical theoretical elastic critical buckling equations and values for each cross-section. An explanation of how the additional terms such as I_w and J, that are required in the theoretical equations is also given.

The theoretical equations provided in Section 2.4.2, which are for unrestrained simply supported T-section columns, serve two purposes.

(i) Firstly, to ensure that the Finite Element Analysis (FEA) modelling and chosen mesh size provide sufficiently accurate results when compared to theoretical elastic critical buckling behaviour, thereby providing reliable results.
(ii) Secondly, to establish a baseline for comparing the effects of different support conditions on the elastic critical buckling loads.

3.2.1 Section Properties

Four T cross-sections with the section properties as shown in Figure 3.1 were used in this study, as shown in Table 3.1

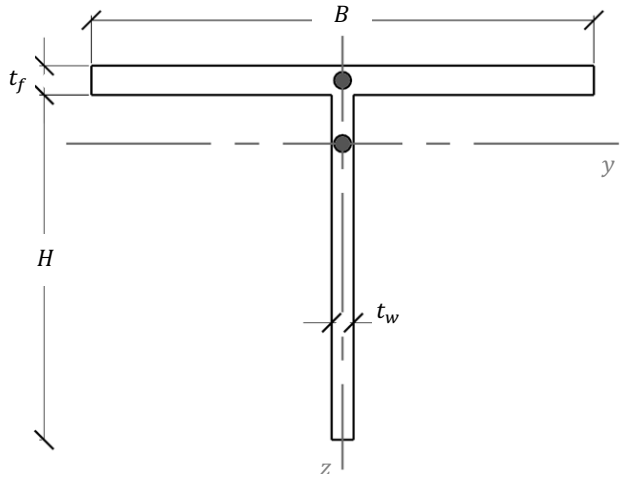

Figure 3.1 – T-Section Dimensional Notation

Table 3.1 - T-Section Dimensions

Section	*H - mm*	*B - mm*	t_f *- mm*	t_w *- mm*
T-1D	99.5	133.5	7.8	5.8
T-2D	191.2	133.5	7.8	5.8
T-3D	282.9	133.5	7.8	5.8
T-4D	374.6	133.5	7.8	5.8

where,

H is the overall depth of the section

B is the width of the flange

t_f is the thickness of the flange

t_w is the thickness of the web

The material properties used in the FE analysis are shown in Table 3.2.

Table 3.2 - Steel Grade S235 Material Properties

E - MPa	*ρ – kgm^{-3}*	*ν*	*G - MPa*	*σ$_o$ – Nmm^{-2}*
214000	7850	0.3	82300	235

where,

E is the Young's modulus

ρ is the material density

ν is the Poisson's ratio

G is the shear modulus

σ_o is the material yield stress

3.2.2 Elastic Critical Flexural and Flexural-Torsional Loads

Additional properties need to be determined to compare the FEA results with those obtained from the theoretical elastic critical buckling equations, as listed in equation 2 - 3, in Section 2.5.2.

SCI P363, (2011) provides the secondary warping constant, I_w, for a T-section as:

$$I_w = \frac{B^3 {t_f}^3}{144} + \frac{(H - {t_f}/{2})^3 \cdot {t_w}^3}{36} \qquad (3 - 1)$$

The torsional constant, J, for any section with an open cross-section can be found using:

$$J = \sum_{i=1}^{n} \left(\frac{B t^3}{3} \right) \qquad (3 - 2)$$

Which, for a T-section, equates to,

$$J = \frac{B {t_f}^3}{3} + \frac{(H - {t_f}/{2}) \cdot {t_w}^3}{3} \qquad (3 - 3)$$

Table 3.3 - Cross-Sectional Properties for Sections T-1D – T-4D

Section	I_y - mm^4	I_z - mm^4	I_w - mm^6	*J* - mm^4
T-1D	1.25 x 10^6	1.55 x 10^6	1.26 x 10^7	27335
T-2D	7.80 x 10^6	1.55 x 10^6	4.35 x 10^7	33299
T-3D	2.27 x 107	1.55 x 10^6	1.26 x 10^8	39263
T-4D	4.84 x 10^7	1.55 x 10^6	2.84 x 10^8	45227

3.2.3 Section Geometric Ratios

Specimen T-1D to T-4D can be seen in Figure 3.2, the section classification of the outstand elements will be dependent on the dimensions from the flange-web junction to the extreme ends of the flange and the web. The ratios for C_w/t_w, C_f/t_f and h/b for sections T-1D to T-4D are listed in Table 3.4.

$$C_w = H - T \qquad (3-5)$$

$$C_f = \frac{B - T_w}{2} \qquad (3-6)$$

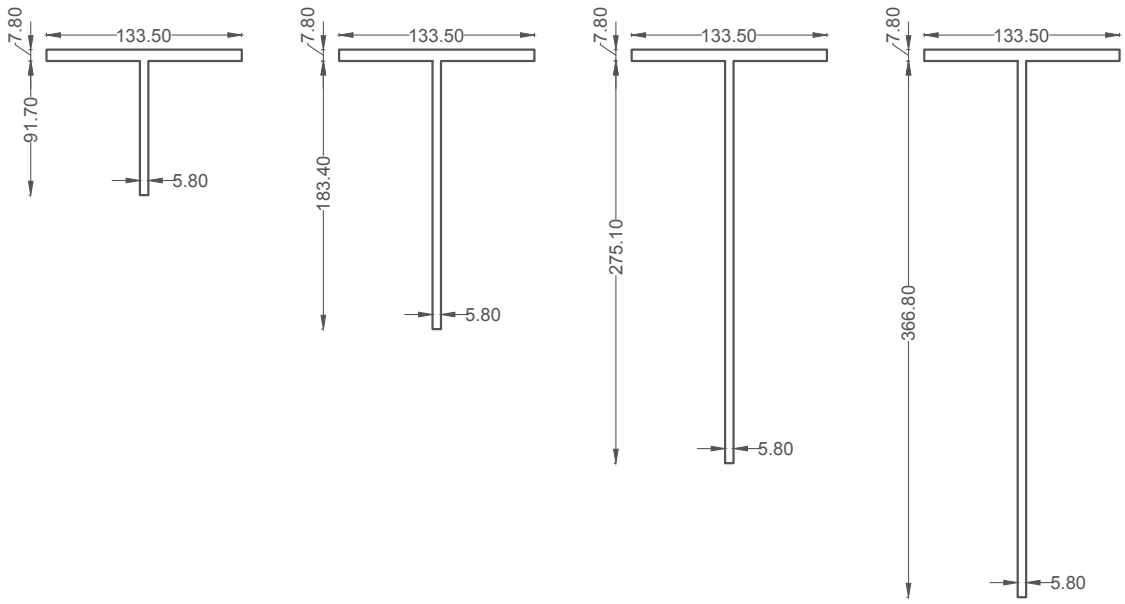

Figure 3.2 – Diagram of Cross-Sections T-1D – T-4D

Table 3.4 - Sections Geometric Ratios

Section	C_w	C_w/t_w	C_f	C_f/t_f	*h/b*
T-1D	91.7	15.81	63.85	8.19	0.75
T-2D	183.4	31.62	63.85	8.19	1.43
T-3D	275.1	47.43	63.85	8.19	2.12
T-4D	366.8	63.24	63.85	8.19	2.81

3.3 Finite Element Modelling

The approach taken for carrying out this parametric study, included applying different web restraining conditions along the free edge of the web, as shown in Figure 1.3. This was done to simulate the behaviour of a T-section that is restrained by other T-sections (Figure 1.4), such as a flanged cruciform section.

The depth of the web was varied, whist all other cross-sectional dimensions were kept constant. This was done to gain an understanding of the restraining effects applied to the free edge of the web. The finite element modelling software package LUSAS (2024) was used for modelling and testing of the various T-sections. The next section explains how the FE models were set up for the different tests that were required.

3.3.1 Geometry

To model the T-section into LUSAS, the geometry was described by five points, as shown in Figure 3.3. These points describe the centreline position of the T-section. Apart from the intersection and the extreme ends of the T section, an additional point was introduced to describe the neutral axis position. After defining the points, they can then be joined by lines. The lines that form the cross-section are then extruded to create the surface representing the length of the different members to be analysed, to which a finite element mesh was applied.

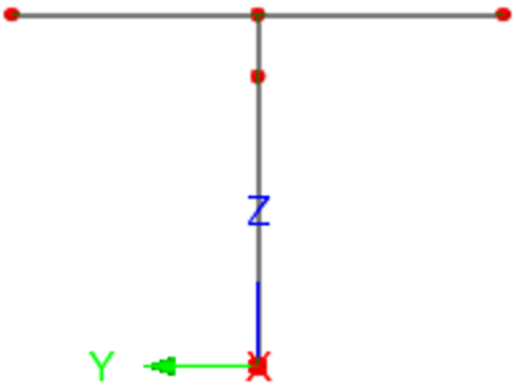

Figure 3.3 – Point Geometry of Model T-1D

The extrusion of these lines occurs in two steps, one at half the member length and the other at the end of the member length, shown in Figure 3.4. This was done to enable the assignment of support conditions to the ends of the member and at the mid-length. The last step in defining the geometry of the T-section involves assigning the flange and web thickness.

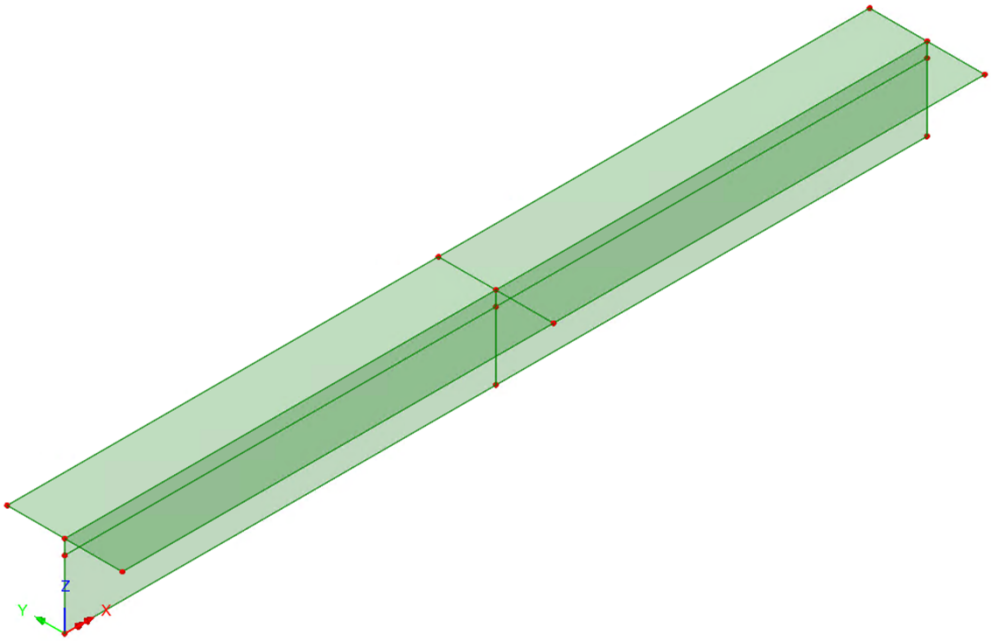

Figure 3.4 – Surfaces Defining Model Length T-1D

3.3.2 Mesh

The mesh can be defined as any number of specified surface subdivisions. To determine an appropriate mesh size, preliminary calibration tests were performed, and the mesh size chosen discretises the member such that each subdivision is approximately 16mm.

Compared to the values obtained using the theoretical elastic critical equations, (equations 2.1 – 2.4) the FE model provides results with an accuracy of less than 5%. A finer mesh size could have been employed; however, the increase in accuracy was minute and not deemed worthy of the additional computing power and time required to run each test.

LUSAS (2024) offers multiple options for different element types, element shapes and interpolation order. The mesh chosen for the models in this study consisted of quadrilateral shape thick shell elements (QTS8) that used a quadratic interpolation order. This configuration was chosen as it proved to be the most accurate configuration for the model.

3.3.3 Material Properties

To simulate a steel material, an elastic isotropic material was defined with a Young's Modulus of 214,000N/mm^2 and a Poisson's ratio of 0.3. This material was then assigned to each surface of the model.

3.3.4 Boundary Support Conditions

Pin-ended support conditions were assumed for the FE models, so that the effective length, L_{eff} would be equal to the actual length of the model. To achieve this, the boundary conditions at both ends of the member required the flange to be restrained from vertical translational movement and the web to be restrained from horizontal translational movement. Whilst at mid-length, the point representing the centre of gravity of the member was restrained in the x-direction. The support conditions described can be seen in Figure 3.5.

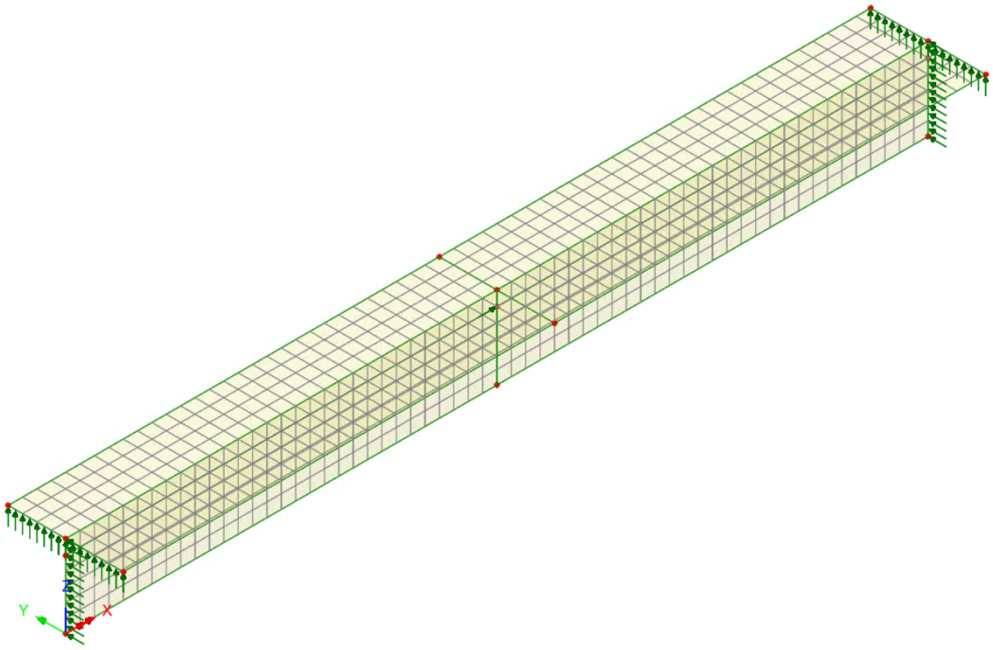

Figure 3.5 – Boundary Conditions applied to Model T-1D

3.4 Load Cases

This study was conducted for two load cases. That is axial loading, and a combined axial and bending stress distribution. This section shall explain how these load cases were achieved and applied to the FE model.

3.4.1 Load Case 1 - Axial Load

For axial loading, a unit axial load of 1 kN needs to be applied to the ends of the member. This was achieved by dividing a 1 kN load applied at each end of the member by its cross-sectional area, yielding a stress value in MPa. The value for stress obtained was then multiplied by the thickness of the flange and the web respectively. The resulting line loads, shown in Table 3.5 were applied accordingly as shown in Figures 3.6.

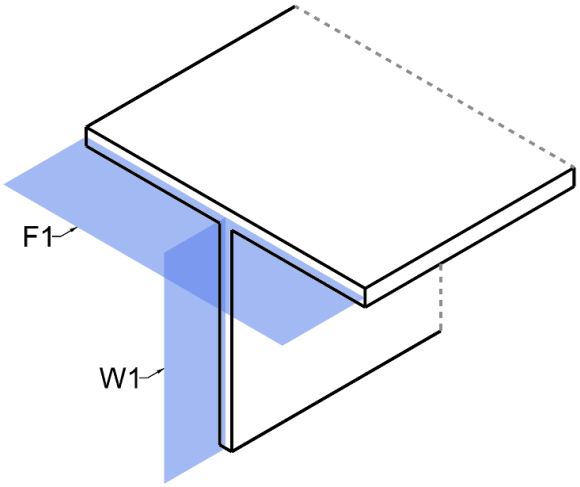

Figure 3.6 – Line Loads representing Load Case 1

Table 3.5 - Line Loads Applied for Load Case 1

Line Load	*Model T-1D*	*Model T-2D*	*Model T-3D*	*Model T-4D*
F1	4.95817 N/mm	3.70543 N/mm	2.95804 N/mm	2.46155 N/mm
W1	3.68685 N/mm	2.75532 N/mm	2.19957 N/mm	1.83038 N/mm

3.4.2 Load Case 2 - Combined Axial Load and Bending Moment

This stress distribution for the second load case being considered, ranges from maximum stress at the top fibre of the top flange to zero at the bottom (the equivalent N.A. position), was applied to simulate the bending behaviour of a compound section, notably the FCS (Figure 3.7), on the T-section. When looking at the behaviour of a compound section, such as an FCS, bent about the horizontal axis, since the centroid of the section lies on the point of symmetry, when undergoing bending, these types of sections will experience an equal value for compressive and tensile stress.

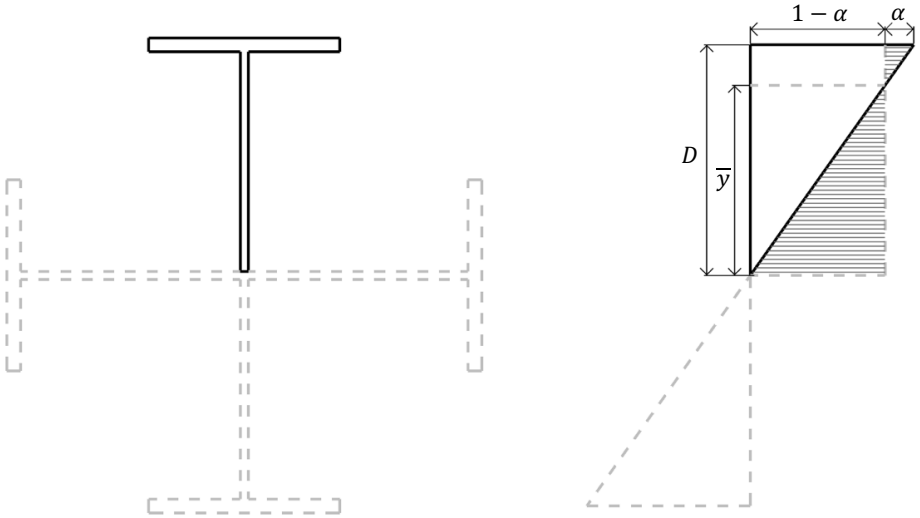

Figure 3.7 – (a) Cruciform Section (b) End Moment

Since the T-section is monosymmetric, it would normally have its neutral axis closer to the flange, on the plane of symmetry. Hence, when attempting to simulate the triangular stress distribution to examine the effect on the T-section, where the free end of the web is laterally restrained against displacement, (i.e., effectively held in position by web restraints). In actuality, the resulting stress distribution is a specific combination of axial and bending stress, as shown in Figures 3.8. The ratio

of axial to bending stress is dependent on the ratio of the depth of the section to the neutral axis position, and although the stress distribution is composed of two types of stresses, the strain at the bottom at the location of the free web is still be expected to be zero.

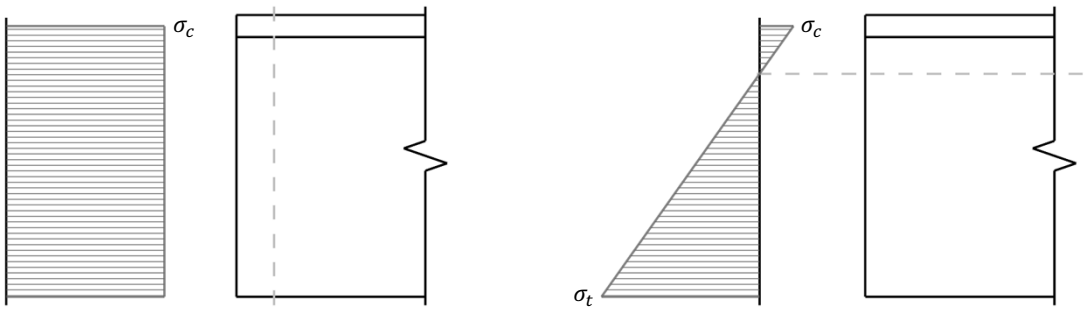

Figure 3.8 – (a) Axial Stress Component (b) Bending Stress Component

To simulate the stress distribution shown in Figure 3.7, on the T-section, a group of line loads acting together were applied, as shown in Figure 3.9. This was achieved by using the equation of flexure to determine the average bending stress at each location along the applied loads and multiplying by the thickness of each element.

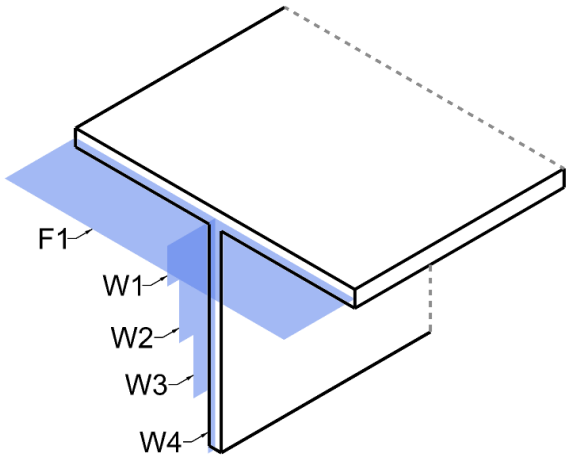

Figure 3.9 – Line Loads representing Load Case 2

The application of these line loads required additional point geometry to be defined in the FE model, as shown in Figure 3.10. This was done by subdividing the distance between the node representing the bottom of the web and the neutral axis into three subdivisions. Therefore, the web is subdivided into four parts in total. The resulting line loads applied to the different parts of the model can be seen in Table 3.6.

Table 3.6 - Line Loads Applied for Load Case 2

Line Load	*Model T-1D*	*Model T-2D*	*Model T-3D*	*Model T-4D*
F1	67.70981 N/mm	30.14628 N/mm	17.93883 N/mm	12.12305 N/mm
W1	45.91923 N/mm	19.52560 N/mm	11.29304 N/mm	7.48560 N/mm
W2	34.57512 N/mm	13.86227 N/mm	7.70579 N/mm	4.96385 N/mm
W3	20.74507 N/mm	8.31736 N/mm	4.62348 N/mm	2.97831 N/mm
W4	6.91502 N/mm	2.77245 N/mm	1.54116 N/mm	0.99277 N/mm

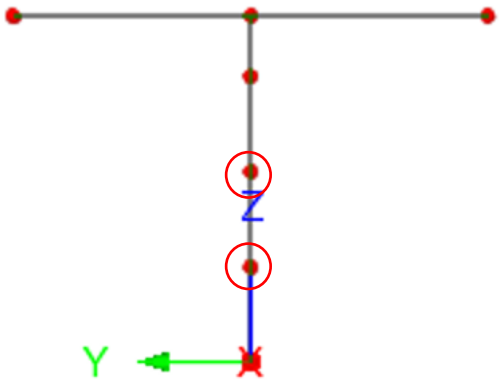

Figure 3.10 – Additional Point Geometry required for Load Case 2

3.5 Web Restraints

The web restraining support conditions, describe in Table 3.7, were applied to the free edge of the web, as shown in Figure 3.11. These restraints were introduced to analyse the behaviour and determine whether these boundary conditions can be related to the behaviour of compound sections.

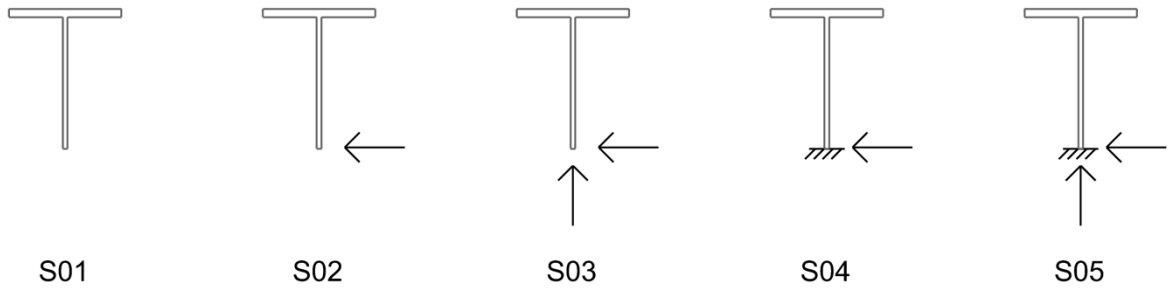

Figure 3.11 – Web Restraining Support Conditions

This progression in longitudinal web edge restraints represents a transition from having the web completely free (S01) to increasing degrees of freedom being restrained (S05), where translational movement in the y and z axes, and rotation about the longitudinal axis are restrained.

Furthermore, the web restraints can be categorised into two categories, where support conditions S02 and S03 can be categorised as in-plane restraints, and S04 and S05 were rotationally restrained.

In every FE model, the end boundary conditions are those of a simply supported member, with an effective length factor of 1.0L, as explained in Section 3.3.4.

Table 3.7 - Definition of Web Restraining Support Conditions

	S01	*S02*	*S03*	*S04*	*S05*
Translation, y		X	X	X	X
Translation, z			X		X
Rotation about, x				X	X

3.6 Elastic Eigenvalue Buckling Analysis

An elastic critical eigenvalue buckling analysis provides the load factor to cause critical buckling for a perfectly straight member. Since the results of the FE analysis are load factors, not the actual load, the applied load must be multiplied by the load factor.

Once the eigenvalue analysis is set to display buckling loads, and a value for the number of eigenvalues is inputted, which for this study was set to 90, the analysis provides the eigenvalues and eigenvectors, for the different buckling modes that may occur. The first eigenvalue represents the predominant critical buckling load and its corresponding buckled mode shape. Subsequent eigenvalues and eigenvectors give the higher load factors and associated mode shapes.

The analysis was carried out for the model explained in Section 3.3, and it was performed for the cross-sections in Table 3.1, for lengths of between 1m to 8m, in steps of 1m. The first three modes of elastic critical buckling of a simply supported T-section are shown in Figure 3.12, 3.13 and 3.14 respectively.

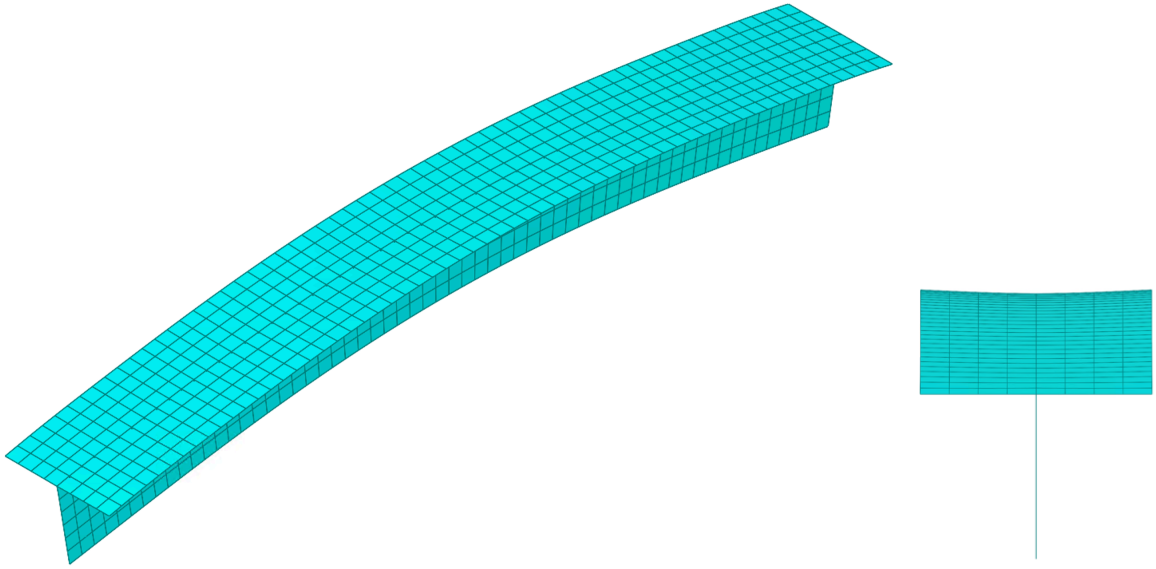

Figure 3.12 - Major-Axis Flexural Buckling (Left) Isometric View, (Right) End View (LUSAS (2024))

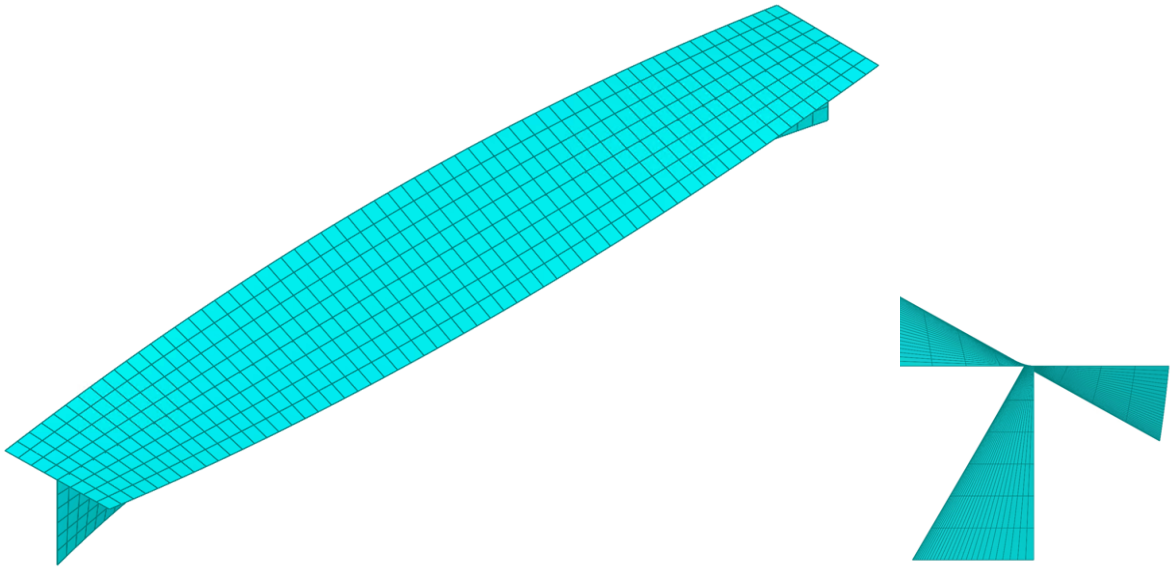

Figure 3.13 - Flexural-Torsional Buckling (Left) Isometric View, (Right) End View (LUSAS (2024))

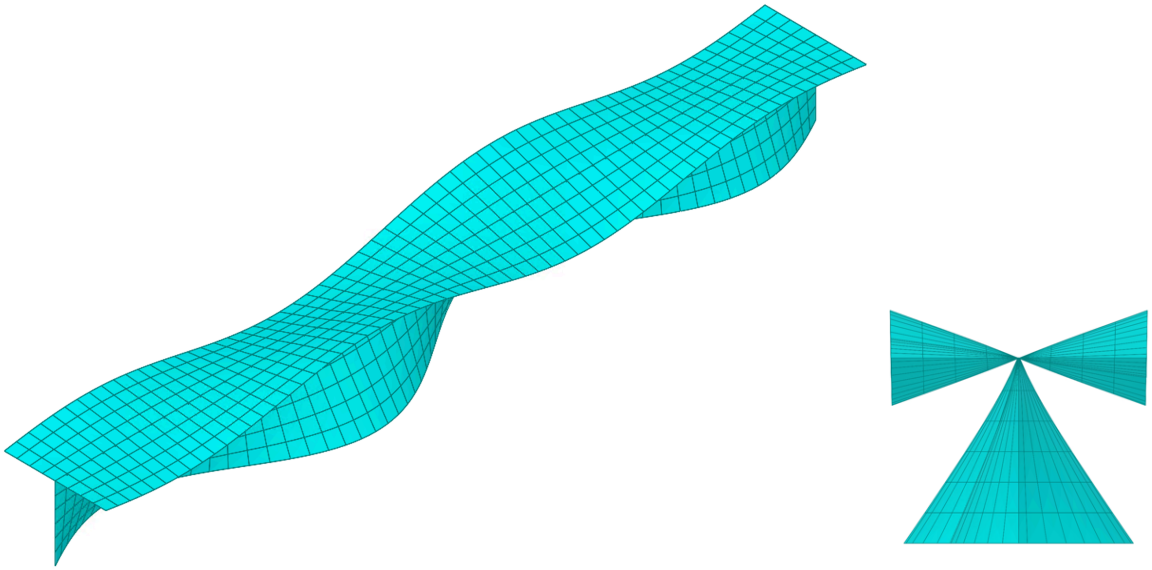

Figure 3.14 - Local Buckling (Left) Isometric View, (Right) End View (LUSAS (2024))

Chapter 4: Results

4.1 Introduction

This chapter shall include a discussion based on the observations made from the results obtained in the FE models and the theoretical equations discussed in section 2.4.2. The results for the FE analyses were obtained for the four different models, as described in Table 3.1, and the five web restraints described in Section 3.5, under two load combinations, as described in Section 3.4.

4.2 Critical Flexural and Flexural-Torsional Equations

Figure 4.1 shows the FE results for the four different T-cross-sections, with increasing web depth, for the member lengths that are simply supported with no in-plane restraints at the free end of the web and flange. Also plotted in Figure 4-1 are the various elastic critical buckling modes as derived from theoretical equations, namely for flexural buckling about the y-axis, $N_{cr,\,y}$, flexural buckling about the z-axis, $N_{cr,\,z}$, torsional buckling, $N_{cr,\,T}$, and the flexural-torsional buckling loads $N_{cr,\,FT1}$ *and* $N_{cr,\,FT2}$. These figures demonstrate that the FE model is in good agreement with these equations, as the percentage difference between the theoretical equations and the FE is less than 5%.

As can be seen in the figure, the torsional buckling load, $N_{cr,\,T}$ and the minor axis buckling mode, $N_{cr,z}$ do not have any FE results. This is because the differential equation for flexural-torsional buckling cannot be decoupled, since the centroid and the shear centre of the monosymmetric cross-section are not coincident.

According to the FE results, in all the depths considered, except for model T-1D, the critical buckling mode observed was the flexural-torsional buckling mode. Whereas for T-1D, the critical buckling mode was that of flexural buckling about the y-axis.

4.3 Finite Element Results

The discussion in this chapter shall be split as follows:

i. A comparison between lateral web restraints S02 and S03.
ii. A comparison between lateral-rotational web restraints S04 and S05.
iii. A discussion on both web restraints for Load Case 1.
iv. A discussion on both web restraints for Load Case 2.

4.3.1 Comparison of In-Plane Web Restraints (S02 and S03)

Figure 4.4 shows the results obtained from models T-1D to T-4D for web support conditions S02 and S03. These results contain the elastic critical buckling modes observed, which were local buckling, torsional buckling, and flexural buckling, respectively. These results also include buckling modes consisting of two half-sine waves.

It can be seen that (Figure 4.4) the local and torsional buckling mode values for both support conditions S02 and S03, are almost identical. This implies that the additional translational restraint in the z-axis had practically no impact on the local and torsional modes. The only difference between the results of the support conditions S02 and S03 is the presence of the flexural buckling mode about the y-axis, which, as expected, was not observed in support condition S03, given the translational restraint.

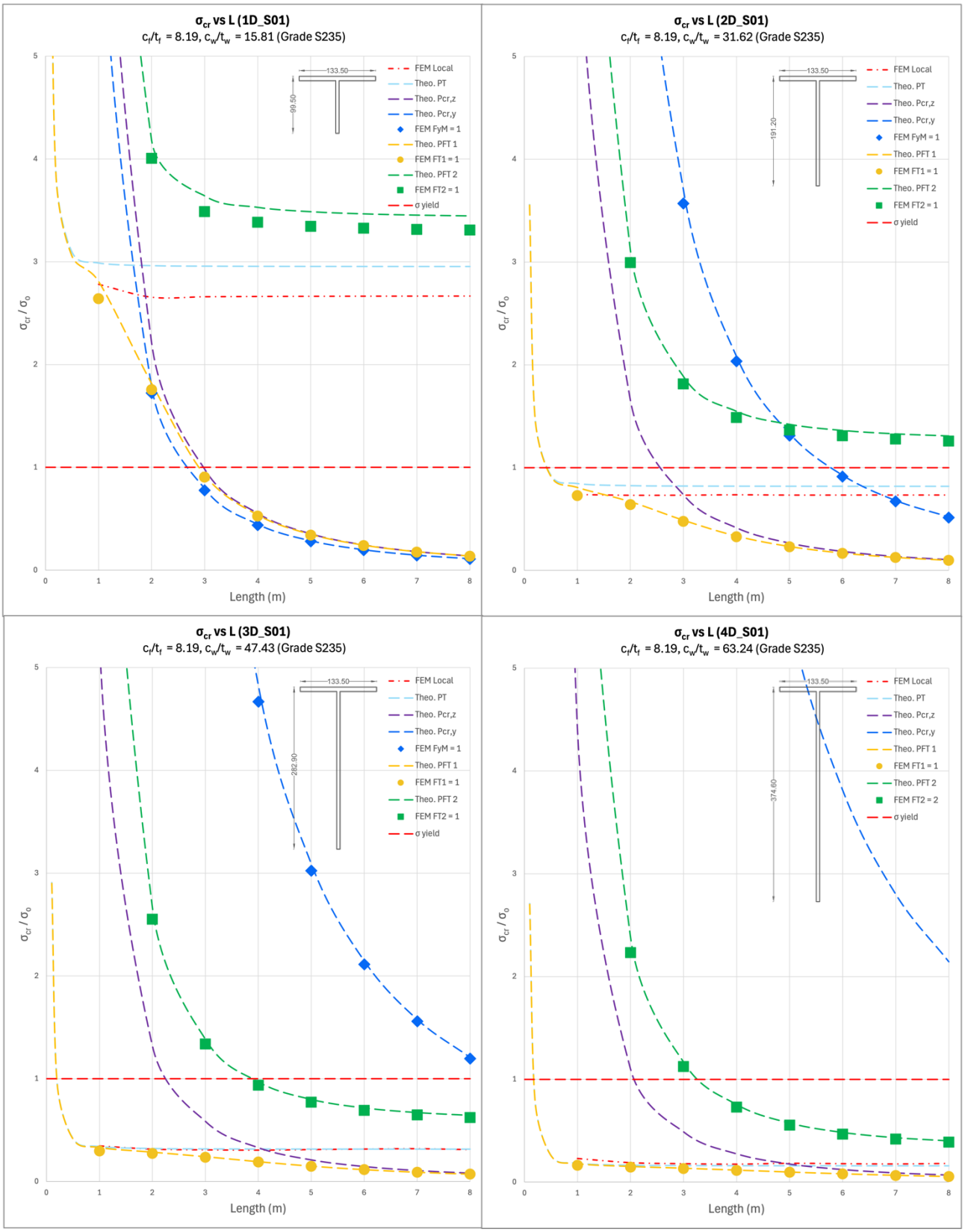

Figure 4.1 - S01 FEM Results vs Theoretical Equations 2-1 to 2-4

Given the objective of this dissertation, that is, to understand how to best predict the elastic critical buckling behaviour of a T-section as if it formed part of a compound section, the web edge boundary conditions that best describe the torsional mode of buckling is support condition S02. This can be observed in the deformed end views of the elastic critical buckled shape in Figure 4.2, across models with varying web depths (T-1D – T-4D). It can be seen that the web of the T-section does not bend and remains straight.

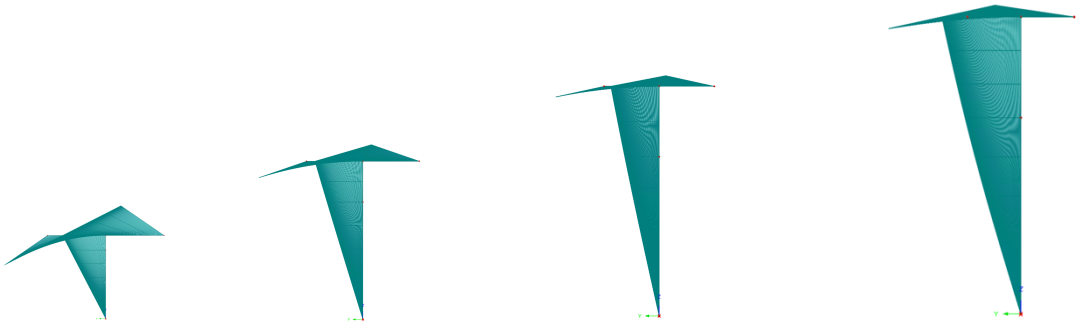

Figure 4.2 - Torsional buckling mode across different web depths (T-1D – T-4D)

4.3.2 Comparison of Rotational Web Restraints (S04 and S05)

Figure 4.5 shows a comparison of rotational web restraint conditions S04 and S05 for the different models tested. Similarly to the previous set of conditions (S02 and S03), there was practically no difference between support conditions S04 and S05 in terms of distortional buckling, and the additional translational restraint in the z-axis does not seem to influence the critical distortional buckling loads. The only difference being that the translational restraint prevents the flexural buckling mode from occurring.

After examining both rotational web edge boundary conditions, S04 and S05, the condition chosen that best describes the distortional buckling mode is support condition S04. This mode of failure is also described in the context of a compound section, as seen in Figure 4.3 for the different cases, T-1D to T-4D analysed. The torsional and distortional buckling modes can be identified from each other by observing the behaviour of the web. In the torsional mode, the web remains relatively straight; in the distortional mode, the web can be seen to be undergoing bending, which is a result of the rotational restraint in the longitudinal axis.

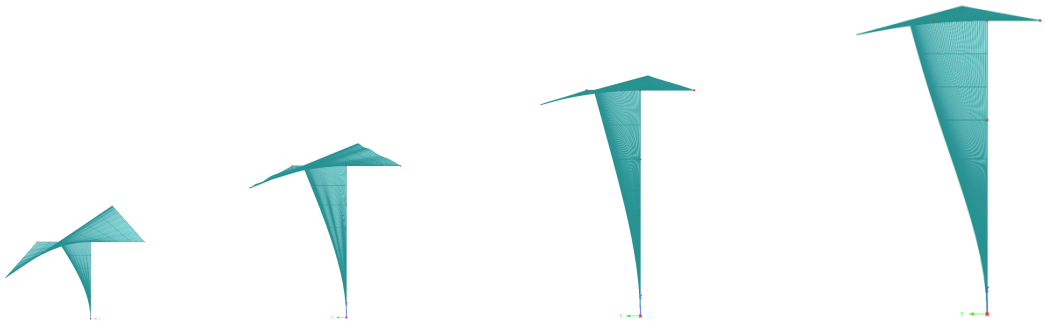

Figure 4.3 - Distortional buckling mode across different web depths (1D – 4D)

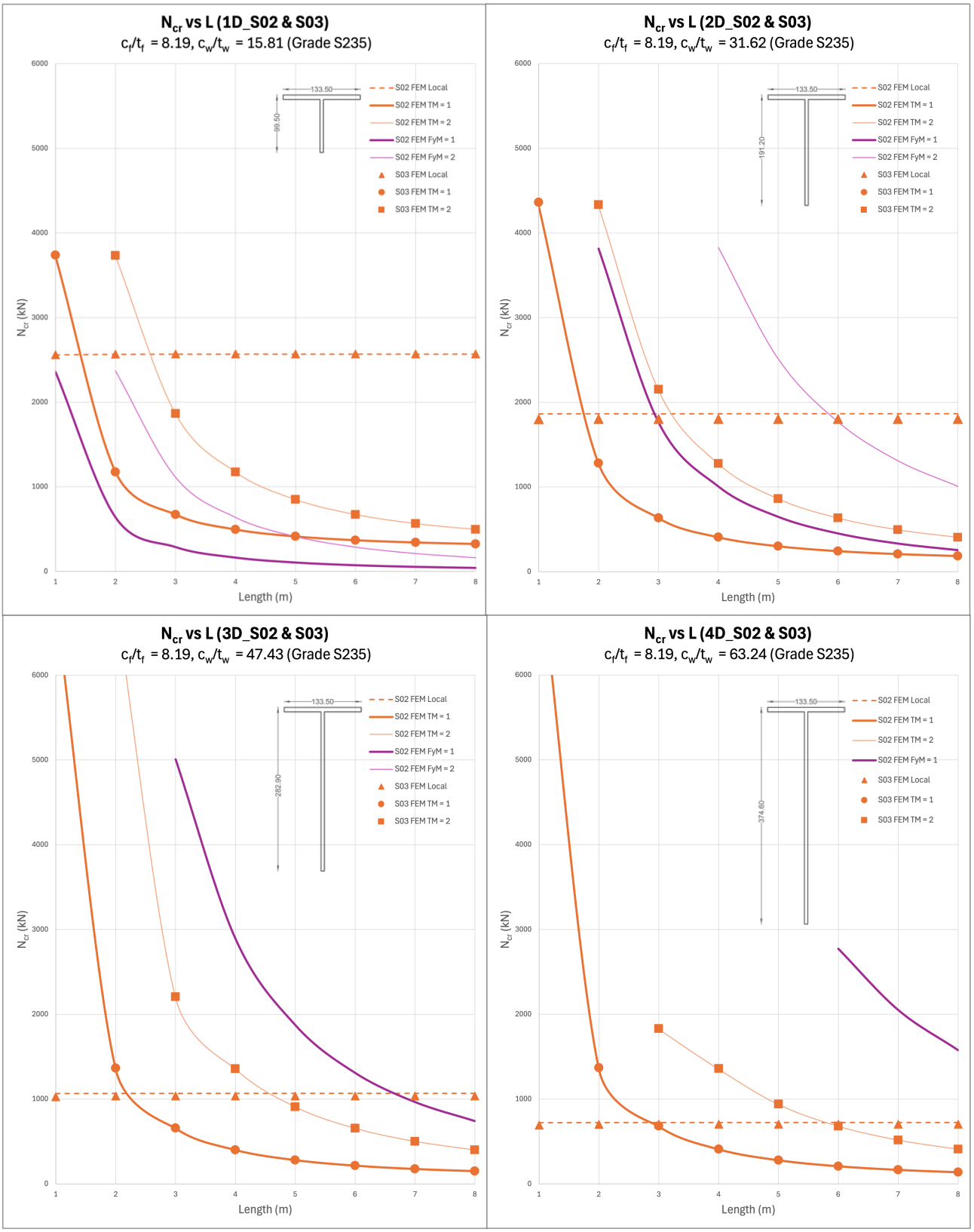

Figure 4.4 - Comparison of Support Conditions S02 and S03 across different depths

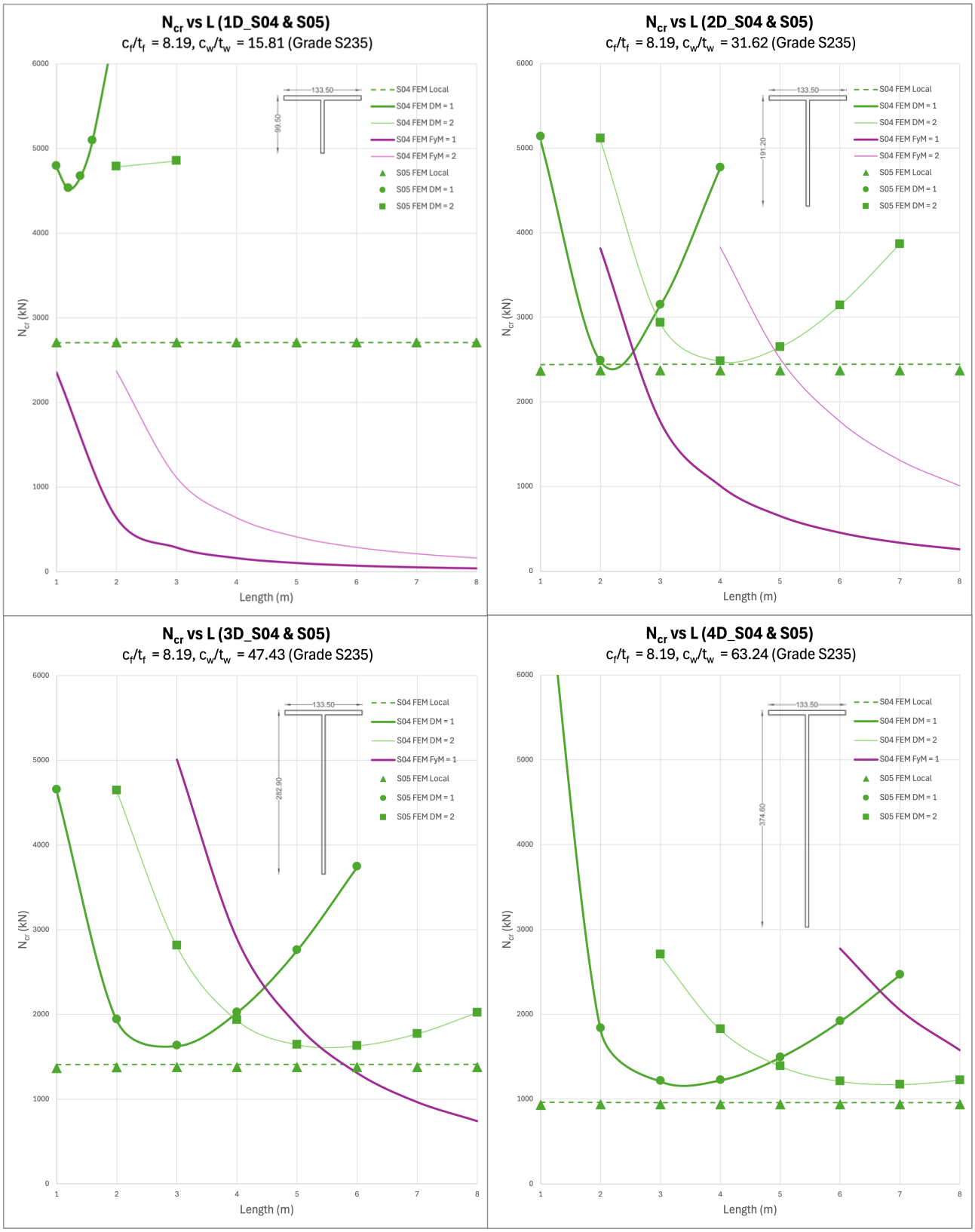

Figure 4.5 - Comparison of Support Conditions S04 and S05 across different depths

4.4 Superimposed Lateral and Rotational Restraints

After reviewing the FE results, it was observed that there is practically no difference between the laterally restrained web edge conditions (S02 and S03), and rotationally restrained web conditions (S04 and S05); with the main difference being the fact that the pure elastic critical flexural buckling modes were not being observed in cases S03 and S05 respectively. Based on this observation, it was decided to use the results from conditions S02 and S04 and base the upcoming discussions on the superimposed results of both the laterally and rotationally restrained web edge boundary conditions.

4.4.1 Observations – Load Case 1

As previously mentioned, the results obtained from the FE analysis are presented as load factors; however, since a load of 1kN was applied, the results can be taken directly from the analysis, where they are converted into a value for critical stress,σ_{cr}, by dividing the critical loads by the area of each cross-section, respectively. The critical stress value is then divided by a design yield stress of 235 MPa, which modifies the y-axis of the graph into a non-dimensional value.

The results for load case 1 have been compiled for both laterally restrained (S02) and rotationally restrained (S04) support conditions, shown in Figures 4-6, 4-8, 4-10 and 4-12. The theoretical elastic critical buckling modes for an unrestrained T-section are also plotted and compared to the FEA results. The results of each model will be discussed for the four models tested, across lengths ranging from 1 m to 8 m.

Comments on Model T-1D (Figure 4 –6)

The FE results for Model T-1D show that for a length greater than 2.6 m, the overall critical elastic buckling mode observed was that of flexural buckling about the y-axis. The second overall mode observed was the torsional mode.

Comments on Model T-2D (Figure 4 –8)

For Model T-2D, the elastic critical buckling mode transitions to the torsional buckling mode for lengths exceeding 3.4 m and remains in this mode thereafter.

Comments on Model T-3D (Figure 4 –10)

Similarly to Model T-2D, the critical buckling mode is the torsional buckling mode for lengths exceeding 3 m. The distortional buckling loads can be seen to significantly decrease when compared to the previous model. In fact, for this model, the distortional buckling load is less than the torsional buckling load for lengths shorter than 1.8 m.

Comments on Model T-4D (Figure 4 –12)

In model T-4D, the local buckling mode for the laterally restrained (S02) support condition has decreased below the yield line. Hence, for the first time, the model fails by local buckling for lengths up to 3m, before reaching the yield stress. The overall elastic critical failure mode is torsional buckling for lengths greater than 3m.

4.4.2 Conclusions – Load Case 1

i. Out of the four models tested, specimen T-1D is the only cross-section where $I_y < I_z$. It is the only specimen where it was observed that flexural buckling in the plane of symmetry was the critical mode, therefore validating theories by Cardoso & Rasmussen, (2013) and Chen, (2007), which predict that for cross-sections with $I_y < I_z$, the critical mode of failure would be flexural buckling about the y-axis.

ii. For both laterally (S02) and rotationally (S04) restrained support conditions, the flexural buckling mode remained consistent in both conditions. Hence, this mode remained consistent with the simply supported condition (S01), and the boundary conditions introduced did not affect this mode.

iii. When analysing the results from one depth to another, the local buckling capacity is seen to decrease as the web depth increases, and the local modes of buckling for the laterally restrained (S02) and rotationally restrained (S04) conditions appear to be converging as the web depth increases. This trend is evident when observing the behaviour across specimens T-2D to T-4D.

iv. As the web depth increases, the length at which the torsional mode starts to occur decreases from 3.4 m in model T-2D and 3 m in model T-3D. In Model T-4D, local buckling occurs before yield, after which the overall torsional mode becomes critical for lengths exceeding 2.9 m.

v. For all the models analysed, the distortional mode never occurs before the local mode, and with the exception of specimen T-3D, the distortional mode never occurs before the torsional mode. This occurrence is uncharacteristic, given that it was the only model where the distortional load was smaller than the torsional load.

vi. Across models T-2D to T-4D, the distortional loads appear to decrease drastically and converges to the torsional loads. This implies a significant interaction between the bending stiffness of the web and the distortional stiffness of the cross-section.

vii. Whilst the torsional stiffness also appears to be decreasing across Models T-1D to T-4D, the rate of decrease is not as drastic as observed for the distortional mode. This implies that the distortional buckling mode is more sensitive to the decrease in web bending stiffness.

viii. For all cases, the values for the elastic critical torsional mode are all contained within the region between the theoretical bounds of the flexural-torsional loads, $N_{FT,1}$, and $N_{FT,2}$.

ix. Whilst the theoretical curves $N_{FT,1}$, and $N_{FT,2}$ seem to be converging, especially at longer member lengths and as the web depth increases, there is a noticeable convergence between the torsional curve and the theoretical $N_{FT,2}$ curve for lengths up to approximately 2 m. This implies that the effect of the EI_w is most significant for lengths up to 2 m, but for lengths longer than 2 m, the effect of the warping, I_w, is less significant, and the effect of GJ is more predominant.

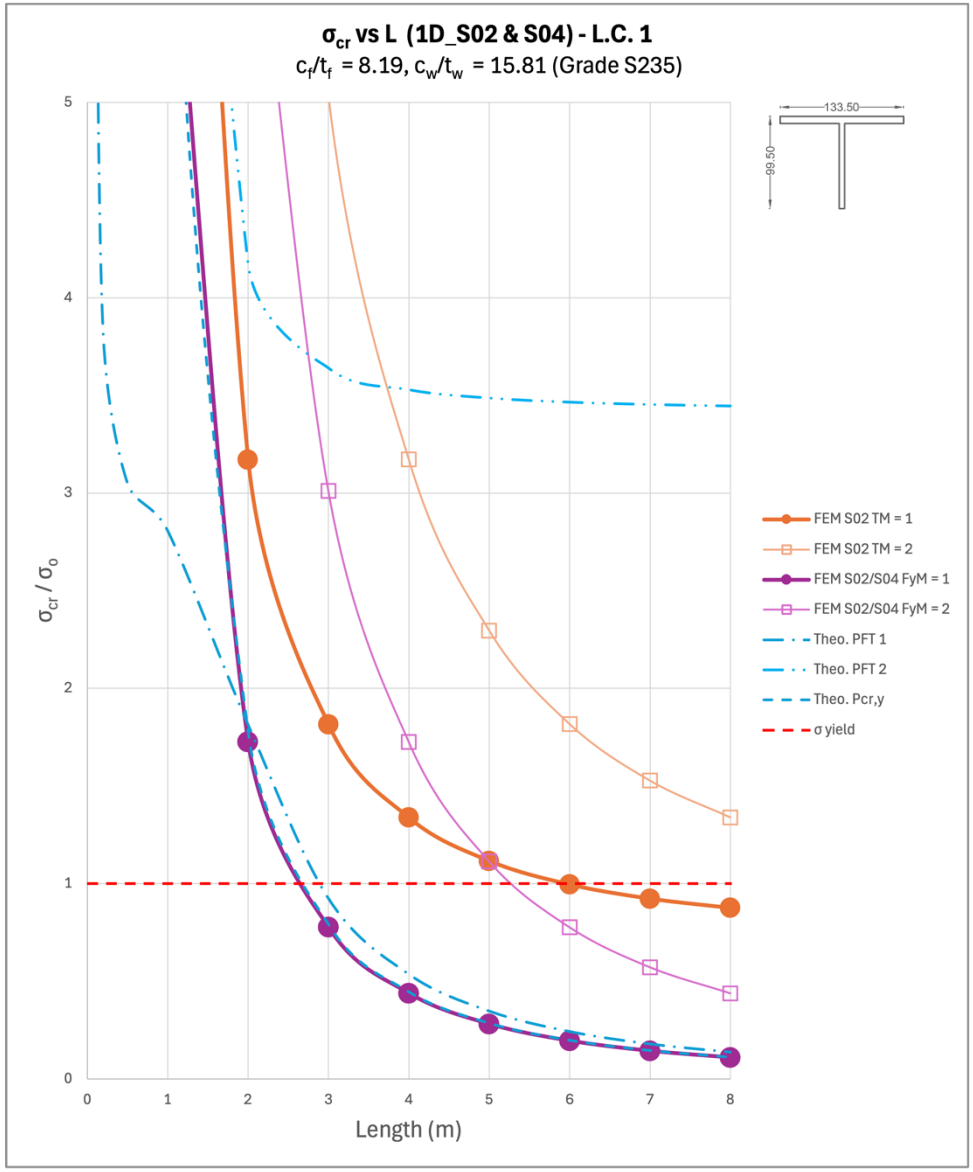

Figure 4.6 - σ_{cr} vs L, Model T-1D_S02 & S04
Load Case 1 (FE vs Theoretical)

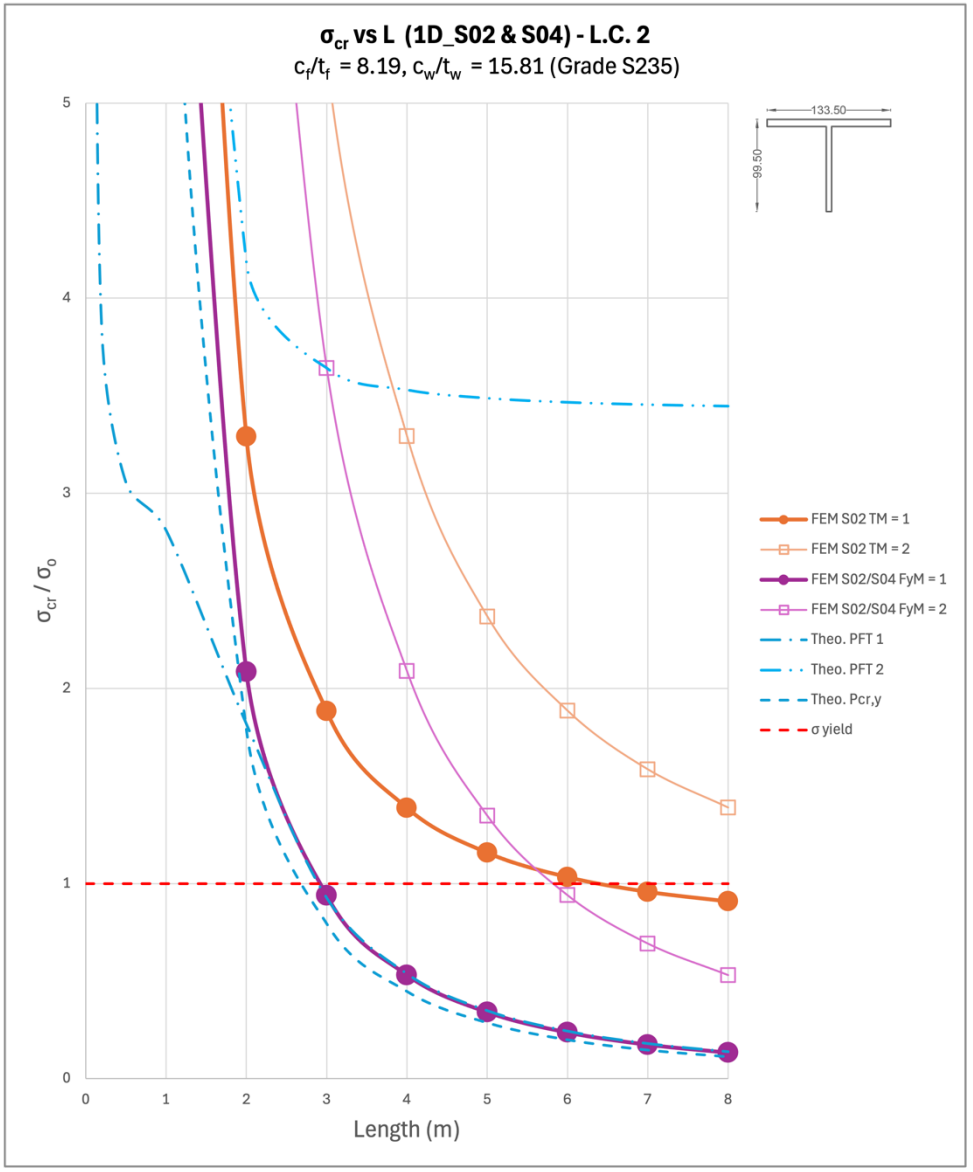

Figure 4.7 - σ_{cr} vs L, Model T-1D_S02 & S04
Load Case 2 (FE vs Theoretical)

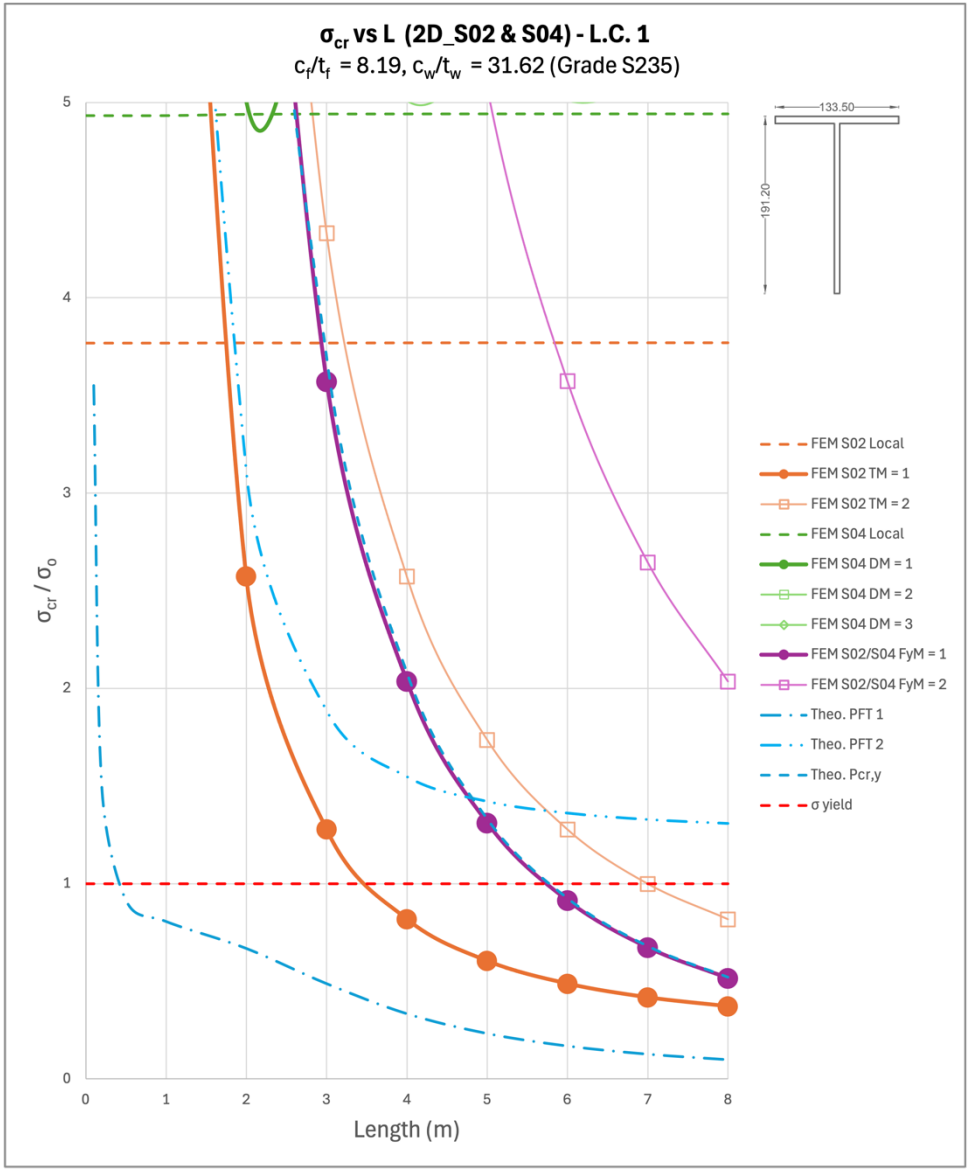

Figure 4.8 - σ_{cr} vs L, Model T-2D_ S02 & S04
Load Case 1 (FE vs Theoretical)

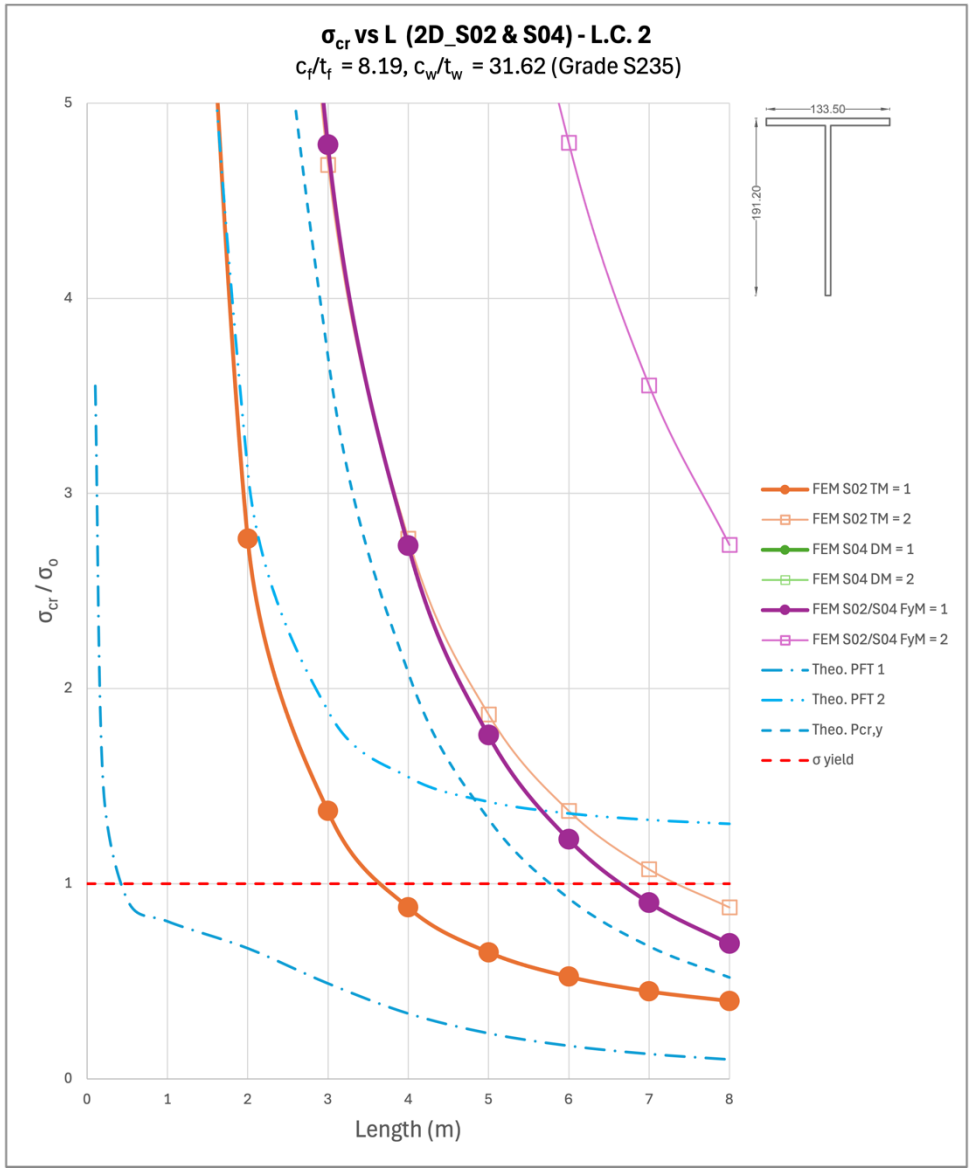

Figure 4.9 - σ_{cr} vs L, Model T-2D_S02 & S04
Load Case 2 (FE vs Theoretical)

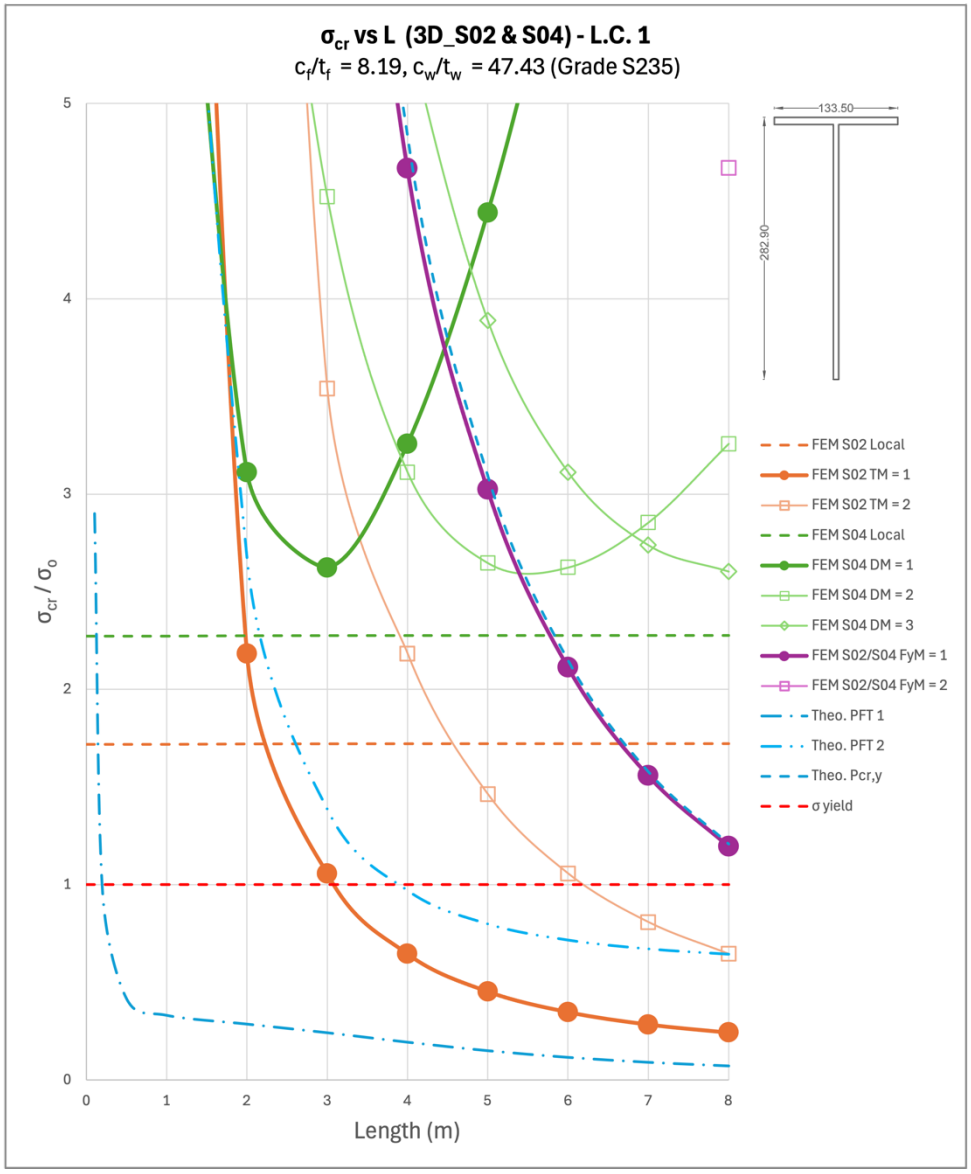

Figure 4.10 - σ_{cr} vs L, Model T-3D_ S02 & S04
Load Case 1 (FE vs Theoretical)

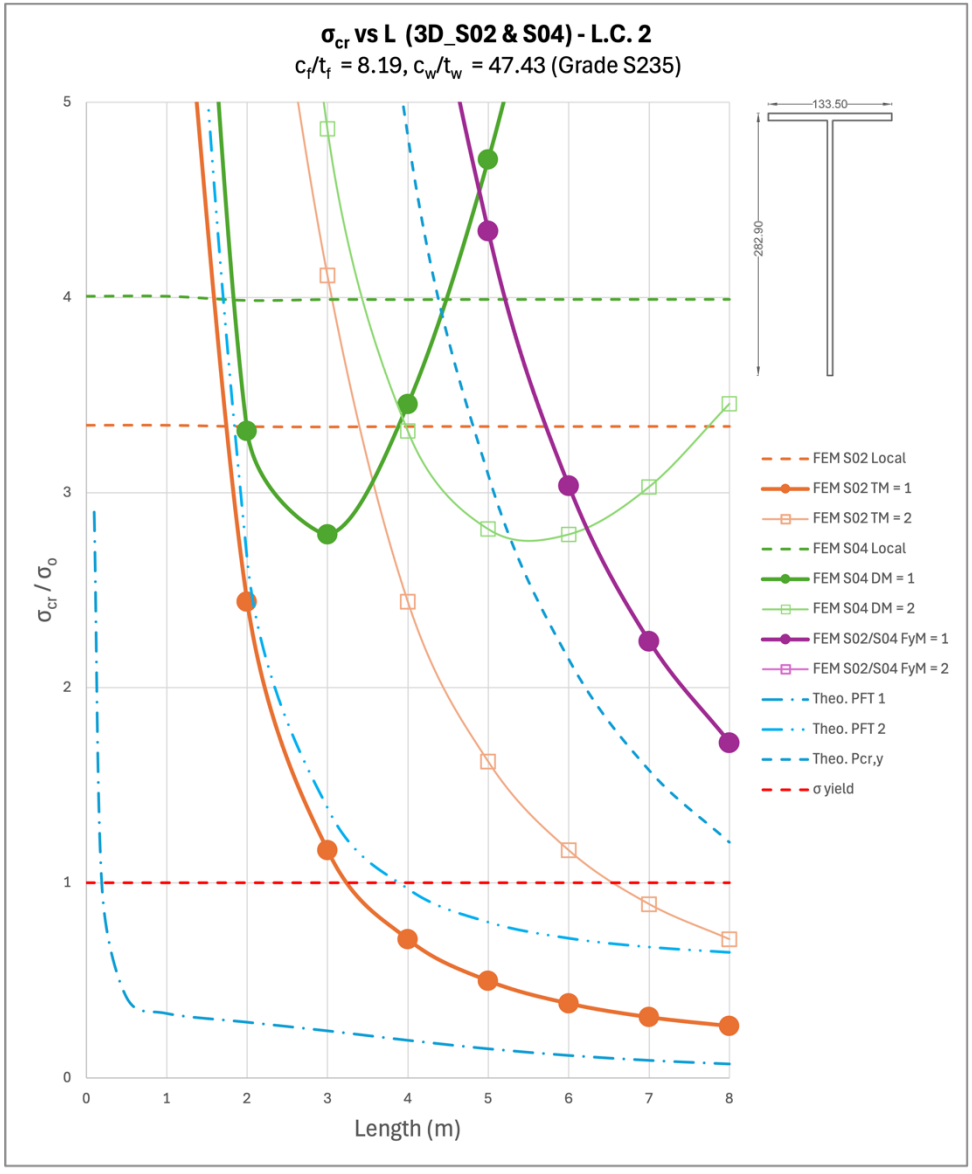

Figure 4.11 - σ_{cr} vs L, Model T-3D_S02 & S04
Load Case 2 (FE vs Theoretical)

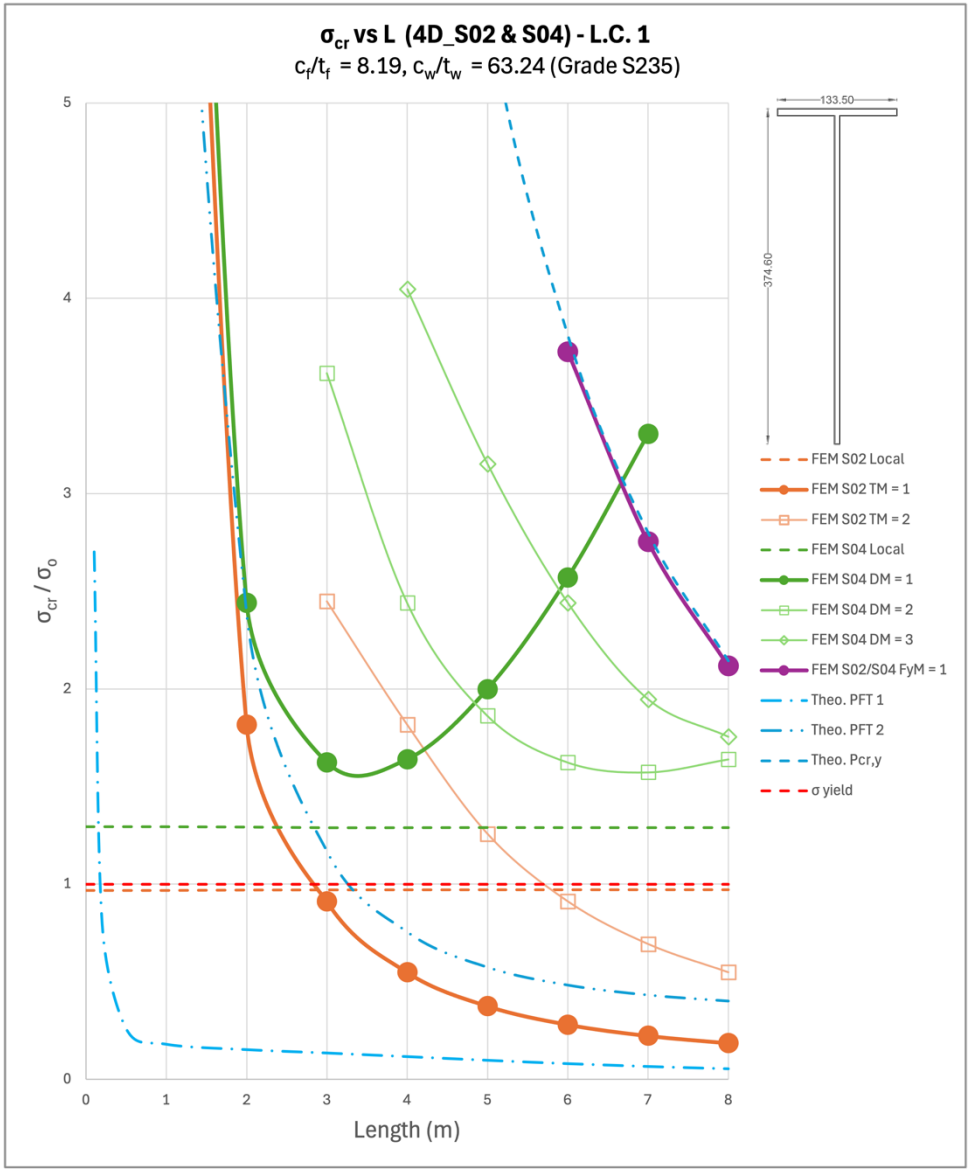

Figure 4.12 - σ_{cr} vs L, Model T-4D_ S02 & S04
Load Case 1 (FE vs Theoretical)

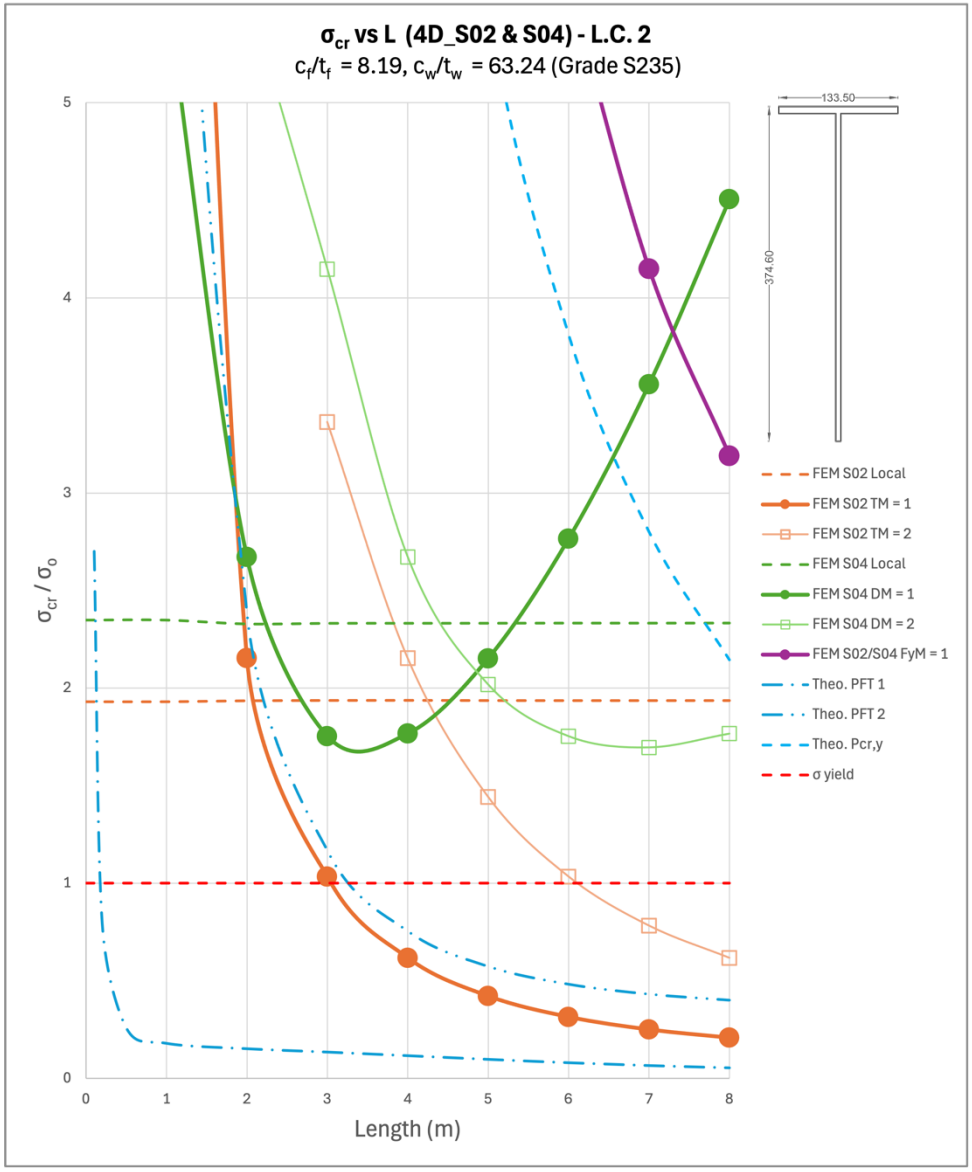

Figure 4.13 - σ_{cr} vs L, Model T-4D_S02 & S04
Load Case 2 (FE vs Theoretical)

4.4.3 Observations – Load Case 2

The FE results for load case 2 are described in this section. As explained in section 3.4.2, the stress distribution being applied in this load case is composed of two stress distributions, that is, an axial component and a bending component. The ratio of the axial load to bending moment applied is dependent on the neutral axis position as defined in Table 4.1. Hence, as the web gets deeper, the position of the neutral axis continues to shift towards the free end of the web, increasing the bending stress. Therefore, if deeper web depths were to be tested, the position of the neutral axis would theoretically start approaching 50% of the total section depth.

Table 4.1 - Load Case 2 Stress Distribution

Section	H	$\bar{y}$	α	% σ_c	% σ_b
T-1D	99.5	78.78	0.21	79%	21%
T-2D	191.2	138.99	0.27	73%	27%
T-3D	282.9	193.41	0.32	68%	32%
T-4D	374.6	244.95	0.35	65%	35%

Comments on Model T-1D (Figure 4 –7)

Similar to the results obtained for Model T-1D under load case 1, the critical overall mode is the flexural buckling about the y-axis and the second overall mode is the torsional mode.

Comments on Model T-2D (Figure 4 –9)

The results for Model T-2D display similar findings to that obtained for load case 1 for this depth, with the main difference being the increase in the flexural buckling loads, which are not being predicted by the theoretical equations.

Comments on Model T-3D (Figure 4 –11)

In Model T-3D, the local buckling modes can be seen to have increased for both lateral and rotational web restraining conditions, which is expected since a non-uniform stress is being applied, and hence the web is less critical to local buckling

Comments on Model T-4D (Figure 4 –13)

In Model T-4D, as expected the critical mode is the torsional mode, however when looking at the behaviour for the critical stress after yield, the distortional mode occurs before the torsional mode, for lengths shorter than 1.9 m.

4.4.4 Conclusions – Load Case 2

i. The observed buckling modes, which are the torsional and distortional buckling modes, are identical to the ones defined in Sections 4.3.2 and 4.3.3, respectively. This is not unexpected given that the majority of the stress components in all the models tested are axial stress.

ii. The critical stress for flexural buckling about the y-axis appears to be increasing, when compared to load case 1, which is expected given the stress distribution being applied.

iii. The critical stress for local buckling for both laterally (S02) and rotationally (S04) restrained conditions is increasing, which is also expected since the stress being applied on the web is less than that applied in load case 1.

iv. As outlined in section 3.4.2, for the stress distribution applied, where maximum stress is being applied at the flange and zero stress being applied at the free edge of the web, zero strain was expected this location. In fact, the FE results confirmed that no axial displacement took place at this location and hence the behaviour of the T-section can be confirmed to behave as if it were part of a compound section, such as the FCS.

Chapter 5: Conclusion

5.1 Conclusions

The first part of this dissertation comprises a literature review based on the behaviour of T-sections, particularly when subjected to axial loading and end moment. Research and experimental data appear to be quite limited for T-sections and FCS, especially when compared to more commonly used sections, such as I and angle sections.

This study investigates the elastic critical buckling behaviour of T-sections, with one of the primary objectives being to develop an approach for simulating the elastic critical buckling behaviour of compound sections by introducing web restraints.

After developing and calibrating the FE model, a parametric study was conducted, analysing four different models with varying web slenderness ratios and member lengths under two load cases and five different web restraining support conditions.

The main observations made from the FE results on models T-1D to T-4D:

i. Across models T-2D to T-4D, the critical stress for the distortional mode appear to decrease drastically. This suggests a significant interaction between the bending stiffness of the web and the distortional stiffness of the cross-section.

ii. In contrast, the torsional mode stays relatively consistent across models T-2D to T-4D, as the web slenderness is increasing. This implies that the bending stiffness of the web has little influence on the torsional stiffness.

iii. A noticeable convergence between the torsional buckling curve and the theoretical $N_{FT,2}$ curve for lengths up to approximately 2 m was observed. This suggests that the effect of the EI_w constant, in equation 2-3, is most significant for lengths up to 2 m, but for lengths longer than 2 m, the effect of the warping, $I_{w,}$ is less significant, and the effect of torsional rigidity, GJ is more predominant.

iv. For the models analysed in this study for both load cases considered, the distortional mode of buckling never occurs before the yield stress, and it was never the critical mode. This suggest that for the practical lengths used in structural designs, the torsional mode is the mode that shall be considered for design.

The main conclusions that can be made based on this study:

i. Introducing the appropriate web restraints to the free edge of the web alters the influence of non-uniform warping torsion.

ii. Based on the FE results and the torsional and distortional buckling modes observed, the influence of warping appears to be primarily dependent on the outer plane stiffness of the flange, which is influenced by the end restraints being applied to the free edge of the web.

iii. To consider the effects of the web restraint being applied, an adjusted formula for predicting the elastic critical torsional buckling load (equation 2-3) shall include an adjusted variable for the warping constant, I_w, where it is calculated about the free edge of the web, not the shear centre of the T-section.

iv. As seen in Figure 5.1, the critical stress values obtained from FE for both the axial load case (load case 1) and the combined axial and bending (load case 2) load cases are in agreement for both the laterally (S02) and rotationally (S04) restrained support conditions. Hence, even for load case 2, where for a T-section the predominant stress is inherently axial, since the same behaviour and buckling modes were observed, it seems that the critical stress may be determined from the same equations as load case 1.

v. When these restraints are applied, other variables might also be influencing the increase in elastic stress. These could include an adjusted value for the torsional constant *J*, since the variables *GJ* in equation 2-3 seem to be affecting the elastic critical stress for longer lengths. An adjusted value for the effective length, L_{eff} might also be a variable that needs to be considered for the formulation of an elastic critical formula, since the increase in warping stiffness might also be affecting the effective length that needs to be considered.

5.2 Further Research

In this dissertation, only the c_w/t_w ratios of the web were varied, this was done by increasing the depth of the web. Ideally, a wider parametric study, including a larger data set with varying section geometric ratios, such as the c_f/t_f ratio for the flange, shall also be examined. This will enable the exploration of the influence of the flange on the torsional stiffness of the cross-section. Hence, critically examining the effects of each component of the T-section, to get closer to critically assessing the behaviour of the T-section under these imposed web restraining conditions.

This dissertation focused on the elastic buckling behaviour of the T-section. Consequently, the next step in the process would involve developing an elastic critical buckling equation for the T-section under various loading conditions. To achieve this, further examination of the magnitude and direction of the end moments applied to the member would be necessary.

Having determined a suitable equation for the elastic critical buckling behaviour of the T-section under bending, a non-linear study of the T-section may be conducted by incorporating the effects of initial imperfections and residual stress patterns, ultimately leading to a better understanding of the ultimate behaviour of compound sections made of T-sections.

Currently, EN1993-1-1 (2005) does not provide any guidelines on how to calculate the elastic critical buckling moment. Therefore, the ultimate aim of the theory presented in this dissertation is to provide initial data that when supplemented with further studies, may lead to an expression for an elastic critical moment formula. This will significantly facilitate structural engineers' design process when designing compound sections.

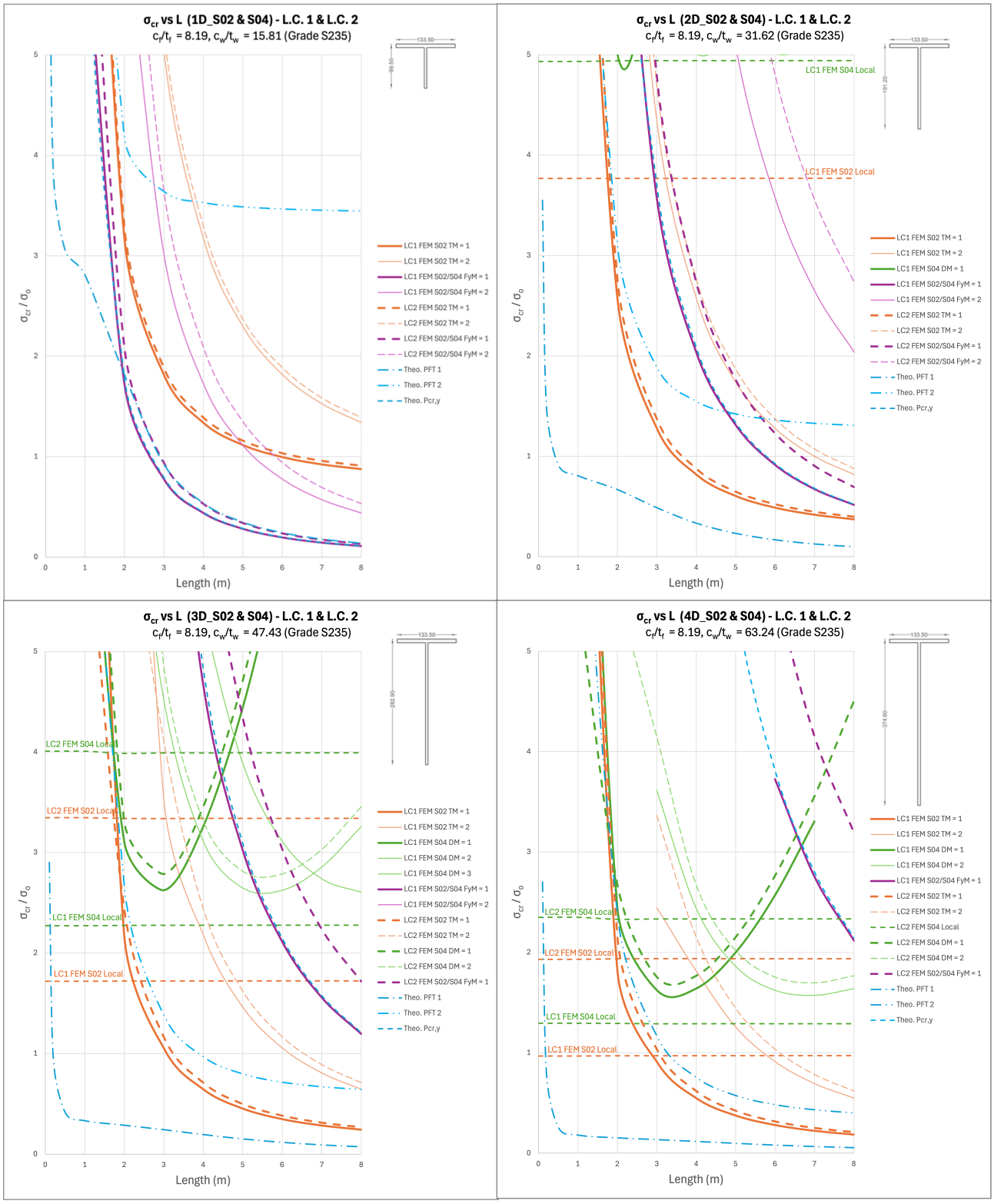

Figure 5.1 - Superimposed Results for Load Case 1 and Load Case 2

Bibliography

Bradford, M. A. (1992). Lateral-distortional buckling of steel I—Section members. *Journal of Constructional Steel Research, 23*(1-3), 97–116.

Bradford, M. A. (1997). Lateral-distortional buckling of continuously restrained columns. *Journal of Constructional Steel Research, 42*(2), 121–139.

Cardoso, F. S., & Rasmussen, K. J. (2013). *THE BEHAVIOUR AND DESIGN OF CONCENTRICALLY LOADED T-SECTION STEEL COLUMNS.*

Dai, R., Behzadi-Sofiani, B., Buhagiar, S., Wadee, M. A., & Gardner, L. (2024). Behaviour, finite element modelling and design of flanged cruciform section steel columns. *Thin-Walled Structures, 204*10.1016/j.tws.2024.112268

Dinis, P. B., Camotim, D., & Silvestre, N. (2010). On the local and global buckling behaviour of angle, T-section and cruciform thin-walled members. *Thin-Walled Structures, 48*(10-11)10.1016/j.tws.2010.04.012

EN 1993-1-1. (2005). *BS EN 1993-1-1 Eurocode 3: Design of steel structures - Part 1-1: General rules and rules for buildings*

Gardner, L., Fieber, A., & Macorini, L. (2019). Formulae for Calculating Elastic Local Buckling Stresses of Full Structural Cross-sections. *Structures, 17*10.1016/j.istruc.2019.01.012

Harris, N., & Urgessa, G. (2018). Strength of Flanged and Plain Cruciform Members. *Advances in Civil Engineering, 2018*(1)10.1155/2018/8417208

Kennedy, J. B., & Murty, M. K. (1972). Buckling of steel angle and tee struts. *Journal of the Structural Division, 98*(11), 2507–2522.

King, C. (2006). *Design of Cruciform Sections using BS 5950-1:2000*. NSC.

Kitipornchai, S., & Lee, H. W. (1986). Inelastic Experiments on Angle and Tee Struts.

Li, L., Fafard, M., & Boissonnade, N. (2022). Local and global instabilities of rolled T-section columns under axial compression. *Thin-Walled Structures, 178*10.1016/j.tws.2022.109517

LUSAS. (2024). *Theory Manual Volume 1*

Naderian, H., Sanches, R., Mercan, O., Kushner, P. J., Azhari, M., & Ronagh, H. (2019). Stability of stiffened cruciform steel columns under shear and compression by the complex finite strip method. *Thin-Walled Structures, 136*10.1016/j.tws.2018.12.023

Schafer, B. W., & Ádány, S. (2005). *Understanding and classifying local, distortional and global buckling in open thin-walled members*

SN003b-EN-EU. (2008). *NCCI: Elastic critical moment for lateral torsional buckling*

SN030a-EN-EU. (2012). *NCCI: Mono-symmetrical uniform members under bending and axial compression*

Steel, T. (2011). P363 Steel Building Design: Design Data. *The Steel Construction Institute and the British Constructional Steelwork Association Limited,*

Tahir, M. M., Shek, P. N., Sulaiman, A., & Tan, C. S. (2008). Experimental investigation of short cruciform columns using universal beam sections. *Construction and Building Materials, 23*(3), 1354. 10.1016/j.conbuildmat.2008.07.014

Taras, A., Kugler, P., & Unterweger, H. (2016). On the behaviour and Eurocode design of T-section columns, beams and beam-columns with slender webs. *Journal of Constructional Steel Research, 129*10.1016/j.jcsr.2016.10.017

Timoshenko, S. P., & Gere, J. M. (1963). *Theory of Elastic Instability (2nd Edition)*. McGraw-Hill International Book Company.

Tohidi, S., & Sharifi, Y. (2014). Restrained distortional buckling capacity of half-through bridge girders. *The IES Journal Part A: Civil &Amp; Structural Engineering, 7*(3)10.1080/19373260.2014.921400

Trahair, N. S. (2013). Post-buckling strength of steel tee columns. *Engineering Structures, 56*, 1800–1807.

Trahair, N. S. (1993). *Flexural-Torsional Buckling of Structures (1st Ed.)*. CRC Press.

Vrcelj, Z., & Bradford, M. A. (2006). Elastic distortional buckling of continuously restrained I-section beam–columns. *Journal of Constructional Steel Research, 62*(3), 223–230

Appendices

Appendix A – Theoretical Elastic Critical Buckling Load Analysis

Table A.1 - Theoretical Critical Loads for Section 1D

$Length\ (m)$	$N_{cr,y}\ (kN)$	$N_{cr,z}\ (kN)$	$N_{cr,T}\ (kN)$	$N_{cr,FT1}(kN)$	$N_{cr,FT2}(kN)$
0.1	263867	326956	2381	379355	2378
0.2	65967	81739	1414	94972	1410
0.5	10555	13078	1143	15355	1129
1	2639	3270	1105	4032	1038
2	660	817	1095	1545	671
3	293	363	1093	1346	342
4	165	204	1092	1305	198
5	106	131	1092	1289	128
6	73	91	1092	1281	90
7	54	67	1092	1277	66
8	41	51	1092	1274	51

Table A.2 - Theoretical Critical Loads for Section 2D

$Length\ (m)$	$N_{cr,y}\ (kN)$	$N_{cr,z}\ (kN)$	$N_{cr,T}\ (kN)$	$N_{cr,FT1}(kN)$	$N_{cr,FT2}(kN)$
0.1	1646576	327271	1760	500236	1757
0.2	411644	81818	743	125220	741
0.5	65863	13091	459	20219	453
1	16466	3273	418	5232	399
2	4116	818	408	1540	331
3	1830	364	406	933	242
4	1029	205	405	765	165
5	659	131	405	703	115
6	457	91	405	673	83
7	336	67	405	657	63
8	257	51	405	647	49

Table A.3 - Theoretical Critical Loads for Section 3D

$Length\ (m)$	$N_{cr,y}\ (kN)$	$N_{cr,z}\ (kN)$	$N_{cr,T}\ (kN)$	$N_{cr,FT1}(kN)$	$N_{cr,FT2}(kN)$
0.1	4789181	327586	1802	590240	1797
0.2	1197295	81896	597	147678	595
0.5	191567	13103	260	23762	258
1	47892	3276	212	6063	206
2	11973	819	200	1653	178
3	5321	364	197	859	150
4	2993	205	197	601	120
5	1916	131	196	495	93
6	1330	91	196	444	72
7	977	67	196	416	57
8	748	51	196	399	45

Table A.4 - Theoretical Critical Loads for Section 4D

$Length\ (m)$	$N_{cr,y}\ (kN)$	$N_{cr,z}\ (kN)$	$N_{cr,T}\ (kN)$	$N_{cr,FT1}(kN)$	$N_{cr,FT2}(kN)$
0.1	10219070	327901	2018	658959	2012
0.2	2554768	81975	593	164829	591
0.5	408763	13116	194	26473	192
1	102191	3279	137	6710	134
2	25548	820	123	1775	114
3	11355	364	120	870	101
4	6387	205	119	562	87
5	4088	131	119	428	73
6	2839	91	118	360	60
7	2086	67	118	322	49
8	1597	51	118	299	41

Appendix B – FE Buckling Modes LUSAS (2024)

Table B.1 - S01_1D Critical Buckling Modes

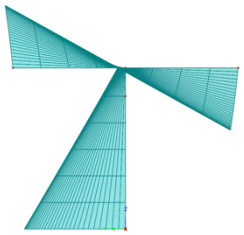 Length = 1 m N_{cr} = 976 kN Local Buckling	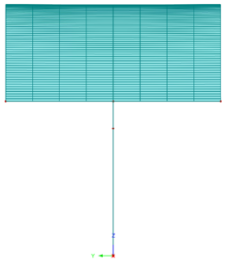 Length = 2 m N_{cr} = 638 kN Flexural Buckling
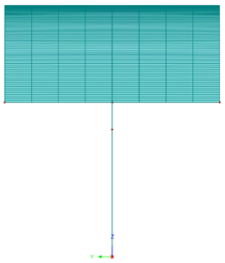 Length = 3 m N_{cr} = 287 kN Flexural Buckling	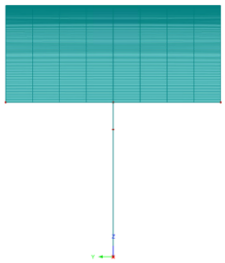 Length = 4 m N_{cr} = 162 kN Flexural Buckling
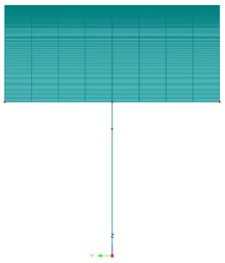 Length = 5 m N_{cr} = 104 kN Flexural Buckling	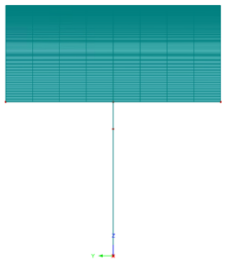 Length = 6 m N_{cr} = 72 kN Flexural Buckling
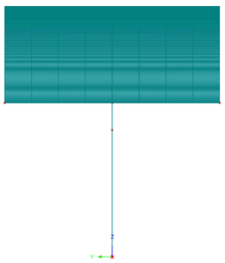 Length = 7 m N_{cr} = 53 kN Flexural Buckling	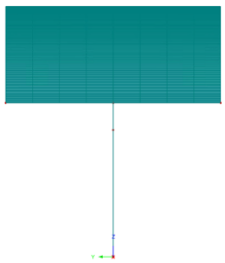 Length = 8 m N_{cr} = 41 kN Flexural Buckling

Table B.2 - S01_2D Critical Buckling Modes

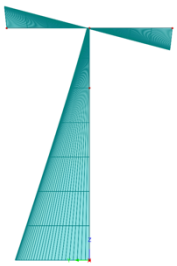 Length = 1 m N_{cr} = 360 kN Flexural-Torsional Buckling	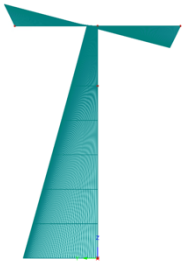 Length = 2 m N_{cr} = 316 kN Flexural-Torsional Buckling
 Length = 3 m N_{cr} = 234 kN Flexural-Torsional Buckling	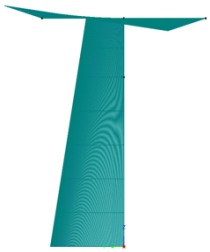 Length = 4 m N_{cr} = 162 kN Flexural-Torsional Buckling
 Length = 5 m N_{cr} = 113 kN Flexural-Torsional Buckling	 Length = 6 m N_{cr} = 82 kN Flexural-Torsional Buckling
 Length = 7 m N_{cr} = 62 kN Flexural-Torsional Buckling	 Length = 8 m N_{cr} = 49 kN Flexural-Torsional Buckling

Table B.3 - S01_3D Critical Buckling Modes

 Length = 1 m N_{cr} = 184 kN Flexural-Torsional Buckling	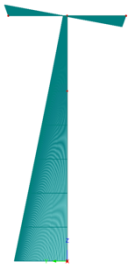 Length = 2 m N_{cr} = 170 kN Flexural-Torsional Buckling
 Length = 3 m N_{cr} = 146 kN Flexural-Torsional Buckling	 Length = 4 m N_{cr} = 118 kN Flexural-Torsional Buckling
 Length = 5 m N_{cr} = 92 kN Flexural-Torsional Buckling	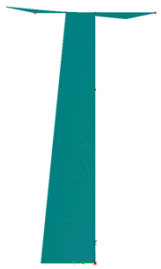 Length = 6 m N_{cr} = 71 kN Flexural-Torsional Buckling
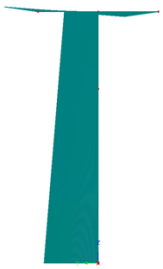 Length = 7 m N_{cr} = 56 kN Flexural-Torsional Buckling	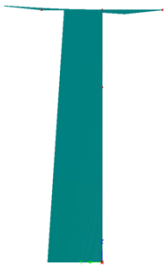 Length = 8 m N_{cr} = 45 kN Flexural-Torsional Buckling

Table B.4 - S01_4D Critical Buckling Modes

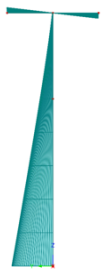 Length = 1 m N_{cr} = 122 kN Flexural-Torsional Buckling	 Length = 2 m N_{cr} = 109 kN Flexural-Torsional Buckling
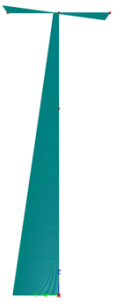 Length = 3 m N_{cr} = 98 kN Flexural-Torsional Buckling	 Length = 4 m N_{cr} = 85 kN Flexural-Torsional Buckling
 Length = 5 m N_{cr} = 72 kN Flexural-Torsional Buckling	 Length = 6 m N_{cr} = 59 kN Flexural-Torsional Buckling
 Length = 7 m N_{cr} = 49 kN Flexural-Torsional Buckling	 Length = 8 m N_{cr} = 40 kN Flexural-Torsional Buckling

Table B.5 - S03_1D Torsional Buckling Modes

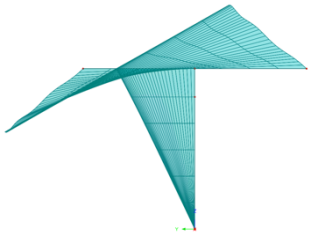 Length = 1 m N_{cr} = 3739 kN Predominantly Torsional buckling	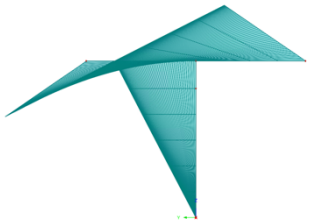 Length = 2 m N_{cr} = 117 5kN Torsional Buckling
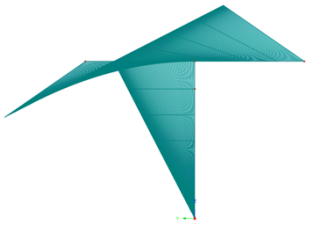 Length = 3 m N_{cr} = 673 kN Torsional Buckling	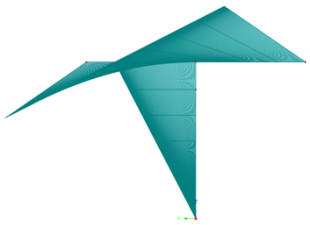 Length = 4 m N_{cr} = 495 kN Torsional Buckling
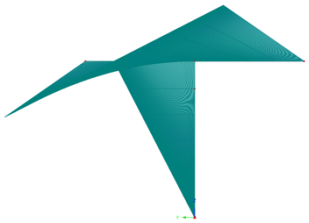 Length = 5 m N_{cr} = 413 kN Torsional Buckling	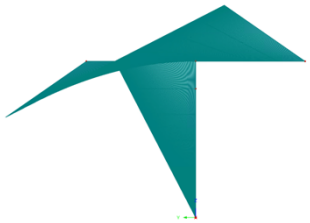 Length = 6 m N_{cr} = 369 kN Torsional Buckling
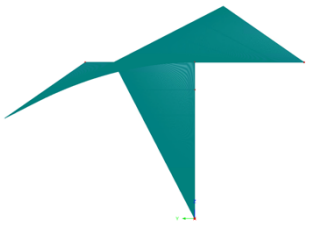 Length = 7 m N_{cr} = 342 kN Torsional Buckling	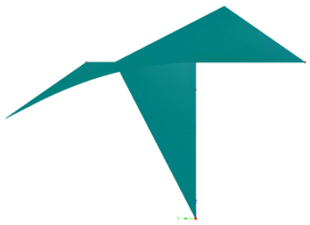 Length = 8 m N_{cr} = 324 kN Torsional Buckling

Table B.6 - S03_2D Torsional Buckling Modes

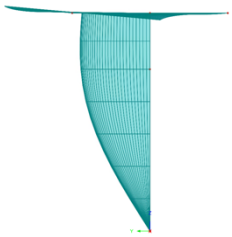 Length = 1 m N_{cr} = 6869 kN Predominantly Torsional Buckling	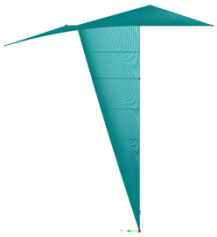 Length = 2 m N_{cr} = 1367 kN Torsional Buckling
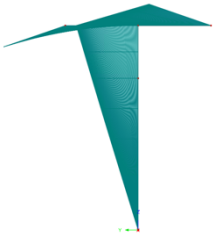 Length = 3 m N_{cr} = 660 kN Torsional Buckling	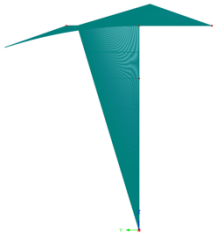 Length = 4 m N_{cr} = 403 kN Torsional Buckling
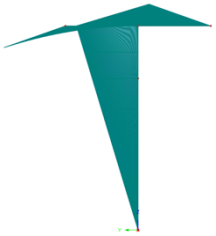 Length = 5 m N_{cr} = 282 kN Torsional Buckling	 Length = 6 m N_{cr} = 216 kN Torsional Buckling
 Length = 7 m N_{cr} = 177 kN Torsional Buckling	 Length = 8 m N_{cr} = 151 kN Torsional Buckling

Table B.7 - S03_3D Torsional Buckling Modes

 Length = 1 m N_{cr} = 6869 kN Predominantly Torsional Buckling	 Length = 2 m N_{cr} = 1367 kN Torsional Buckling
 Length = 3 m N_{cr} = 660 kN Torsional Buckling	 Length = 4 m N_{cr} = 403 kN Torsional Buckling
 Length = 5 m N_{cr} = 282 kN Torsional Buckling	 Length = 6 m N_{cr} = 216 kN Torsional Buckling
 Length = 7 m N_{cr} = 177 kN Torsional Buckling	 Length = 8 m N_{cr} = 151 kN Torsional Buckling

Table B.8 - S03_4D Torsional Buckling Modes

 Length = 1 m N_{cr} = 7415 kN Predominantly Torsional Buckling	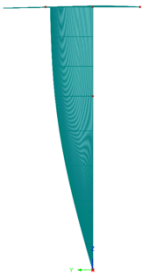 Length = 2 m N_{cr} = 1370 kN Torsional Buckling
 Length = 3 m N_{cr} = 685 kN Torsional Buckling	 Length = 4 m N_{cr} = 411 kN Torsional Buckling
 Length = 5 m N_{cr} = 281 kN Torsional Buckling	 Length = 6 m N_{cr} = 210 kN Torsional Buckling
 Length = 7 m N_{cr} = 167 kN Torsional Buckling	 Length = 8 m N_{cr} = 139 kN Torsional Buckling

Table B.9 - S05_1D Distortional Buckling Modes

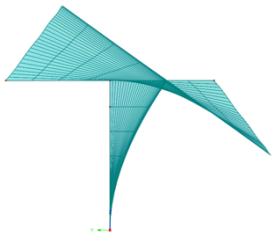 Length = 1 m N_{cr} = 4799 kN Distortional Buckling	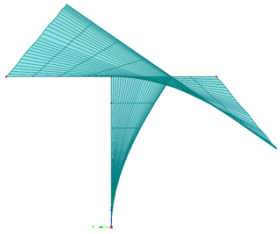 Length = 1.2 m N_{cr} = 4538 kN Distortional Buckling
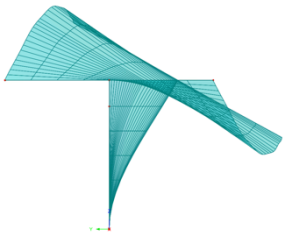 Length = 1.4 m N_{cr} = 4679 kN Predominantly Distortional Buckling	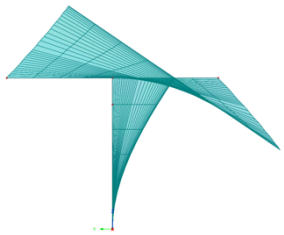 Length = 1.6 m N_{cr} = 5101 kN Distortional Buckling

Table B.10 - S05_2D Distortional Buckling Modes

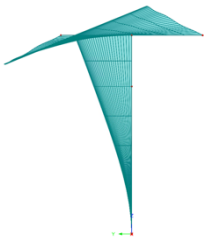 Length = 1 m N_{cr} = 5143 kN Distortional Buckling	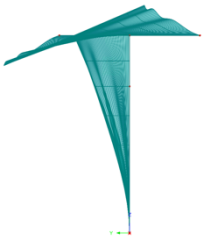 Length = 2 m N_{cr} = 2493 kN Predominantly Distortional Buckling
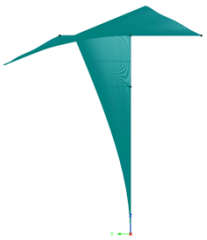 Length = 3 m N_{cr} = 3153 kN Distortional Buckling	 Length = 4 m N_{cr} = 4776 kN Predominantly Distortional Buckling

Table B.11 - S05_3D Distortional Buckling Modes

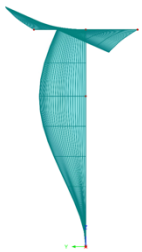 Length = 1 m N_{cr} = 4659 kN Predominantly Distortional Buckling	 Length = 2 m N_{cr} = 1946 kN Predominantly Distortional Buckling
 Length = 3 m N_{cr} = 1638 kN Distortional Buckling	 Length = 4 m N_{cr} = 2029 kN Distortional Buckling
 Length = 5 m N_{cr} = 2765 kN Distortional Buckling	 Length = 6 m N_{cr} = 3749 kN Distortional Buckling

Table B.12 - S05_4D Distortional Buckling Modes

 Length = 1 m N_{cr} = 7869 kN Predominantly Distortional Buckling	 Length = 2 m N_{cr} = 1841 kN Distortional Buckling
 Length = 3 m N_{cr} = 1221 kN Distortional Buckling	 Length = 4 m N_{cr} = 1230 kN Distortional Buckling
 Length = 5 m N_{cr} = 1498 kN Distortional Buckling	 Length = 6 m N_{cr} = 1924 kN Distortional Buckling
 Length = 7 m N_{cr} = 2472 kN Distortional Buckling	